

RESEARCH ARTICLE

A Numerically Subdominant CD8 T Cell Response to Matrix Protein of Respiratory Syncytial Virus Controls Infection with Limited Immunopathology

Jie Liu^{1*}, Elias K. Haddad², Joshua Marceau¹, Kaitlyn M. Morabito¹, Srinivas S. Rao¹, Ali Filali-Mouhim³, Rafick-Pierre Sekaly⁴, Barney S. Graham^{1*}

1 Vaccine Research Center, National Institute of Allergy and Infectious Disease, National Institutes of Health, Bethesda, Maryland, United States of America, **2** Drexel University, Division of Infectious Diseases and HIV Medicine, Philadelphia, Pennsylvania, United States of America, **3** Department of Pathology, Case Western Reserve University, Cleveland, Ohio, United States of America, **4** Center for AIDS Research, Case Western Reserve University, Cleveland, Ohio, United States of America

* jieliu@mail.nih.gov (JL); bgraham@nih.gov (BSG)



 OPEN ACCESS

Citation: Liu J, Haddad EK, Marceau J, Morabito KM, Rao SS, Filali-Mouhim A, et al. (2016) A Numerically Subdominant CD8 T Cell Response to Matrix Protein of Respiratory Syncytial Virus Controls Infection with Limited Immunopathology. *PLoS Pathog* 12(3): e1005486. doi:10.1371/journal.ppat.1005486

Editor: Paul G. Thomas, St. Jude Children's Research Hospital, UNITED STATES

Received: September 25, 2015

Accepted: February 10, 2016

Published: March 4, 2016

Copyright: This is an open access article, free of all copyright, and may be freely reproduced, distributed, transmitted, modified, built upon, or otherwise used by anyone for any lawful purpose. The work is made available under the [Creative Commons CC0](http://creativecommons.org/licenses/by/4.0/) public domain dedication.

Data Availability Statement: All relevant data are within the paper and its Supporting Information files.

Funding: This work was supported by intramural research program awarded to BSG by the National Institute of Allergy and Infectious Diseases of the National Institute of Health (<http://www.niaid.nih.gov/researchfunding/Pages/default.aspx>). The funders had no role in study design, data collection and analysis, decision to publish, or preparation of the manuscript.

Abstract

CD8 T cells are involved in pathogen clearance and infection-induced pathology in respiratory syncytial virus (RSV) infection. Studying bulk responses masks the contribution of individual CD8 T cell subsets to protective immunity and immunopathology. In particular, the roles of subdominant responses that are potentially beneficial to the host are rarely appreciated when the focus is on magnitude instead of quality of response. Here, by evaluating CD8 T cell responses in CB6F1 hybrid mice, in which multiple epitopes are recognized, we found that a numerically subdominant CD8 T cell response against D^bM₁₈₇ epitope of the virus matrix protein expressed high avidity TCR and enhanced signaling pathways associated with CD8 T cell effector functions. Each D^bM₁₈₇ T effector cell lysed more infected targets on a per cell basis than the numerically dominant K^dM₂₈₂ T cells, and controlled virus replication more efficiently with less pulmonary inflammation and illness than the previously well-characterized K^dM₂₈₂ T cell response. Our data suggest that the clinical outcome of viral infections is determined by the integrated functional properties of a variety of responding CD8 T cells, and that the highest magnitude response may not necessarily be the best in terms of benefit to the host. Understanding how to induce highly efficient and functional T cells would inform strategies for designing vaccines intended to provide T cell-mediated immunity.

Author Summary

CD8 T cells play a key role in RSV clearance, immunopathology and disease. Therefore, CD8 T cells can help or harm the host depending on their timing, magnitude, and function. The CD8 T cell response represents a heterogeneous population of cells with

Competing Interests: The authors have declared that no competing interests exist.

phenotypically and functionally diverse subsets, and needs to at least be studied at the level of epitope specificity to understand how to diminish the risk of immunopathology. Studying the bulk response masks distinct contributions of individual CD8 T subsets to immunity and immunopathology. Focusing on CD8 T cell response with the highest magnitude overlooks role of subdominant responses. Here, we studied response to different epitopes and revealed that a numerically subdominant CD8 T cell response against D^bM₁₈₇ epitope of the virus matrix protein controlled virus replication efficiently with limited pulmonary inflammation and illness compared to the previously well-characterized and numerically dominant K^dM₂₈₂ T cell response. Our data show that selectively boosting of epitope-specific CD8 T cell responses may be more beneficial than indiscriminant boosting of all available epitopes to achieve rapid viral clearance while limiting immunopathology. This work has implications for antigen design of vaccines intended to induce T-cell-mediated immunity.

Introduction

Respiratory syncytial virus (RSV) induces robust CD8 T cell responses that play a critical role in controlling virus replication and determining the progression of disease in animal models and infected humans. For example, autopsies of children with fatal RSV infections show a relative deficiency of CD8 T cell responses[1]; recipients of allogeneic bone marrow and lung transplants have difficulty in controlling RSV replication and often have fatal outcomes as a consequence of syncytium-forming pneumonia[2, 3]; and in patients with severe combined immunodeficiency (SCID), RSV infection results in persistent virus shedding that can be controlled with T cell reconstitution[4, 5]. Adoptive transfer of effector CD8 T cells can clear persistent RSV shedding in immunodeficient mice[6]; and depletion of T cells in mice results in persistence of the virus[7, 8]. However, the effect of CD8 T cell responses is not always beneficial. While T cell reconstitution reduces RSV load in SCID patients, it causes significant pulmonary inflammation[5]. In mice, passive transfer of a large amount of CD8 T cells in the setting of RSV infection results in hemorrhagic pneumonia[6], while depletion of CD8 T cells reduces disease severity[7]. Achieving an acceptable balance between protective immunity and immunopathology has been an elusive goal for RSV vaccine development and is a key objective for programs developing preventive and therapeutic strategies for pathogens requiring T cell-mediated immunity.

CD8 T cells are a heterogeneous population with phenotypically and functionally diverse subsets, and viral infection often induces a broad spectrum of CD8 T cell responses[9, 10]. Most studies report bulk CD8 T cell responses, or are focused on CD8 T cells targeting a relatively small number of epitopes. Those immunodominant epitopes are often discovered and selected as endpoints in evaluation of vaccination and immune intervention. Quantitative assessment of bulk CD8 T cell responses has shown little correlation with control of virus replication, and numerically subdominant T-cell responses have been demonstrated to play important roles in immunity against selected viral infections[11, 12], particularly in settings where multiple epitopes are recognized or where immune escape mutations are common[13]. Therefore, it is important to characterize CD8 T cell responses not only by magnitude, but also by functional properties, breadth, location, durability, and contribution to viral clearance and immunopathology.

We took advantage of the CB6F1 hybrid mouse model to characterize CD8 T cell subsets and their role in response to RSV infection. Although semi-permissive, mice infected by

intranasal inoculation of RSV generate robust T cell and antibody responses, and pulmonary inflammation. The kinetics of virus replication and progression of the disease is highly reproducible [14–16]. In CB6F1 mice, the dominant CD8 T cell responses of each parent strain assume a distinct hierarchy, in which response to H2-D^b-restricted M₁₈₇₋₁₉₅ epitope (D^bM₁₈₇) is numerically subdominant to response to the H2-K^d-restricted M₂₈₂₋₉₀ epitope (K^dM₂₈₂) [17]. The numerically dominant K^dM₂₈₂ T cell response lyses RSV-infected cells and reduces viral load, but is also associated with infection-induced immunopathology and severe illness [18, 19]. Mutating this epitope leads to reduced disease and pathology [20]. This observation suggested that this high magnitude and easily measurable response may do more harm than good, and that other subdominant responses could effectively clear virus with less immunopathology. Here, we defined the attributes of the numerically subdominant D^bM₁₈₇ T cell response that targets the RSV matrix protein. We compared the cytotoxicity and control of virus replication, as well as the associated lung pathology and illness to that associated with K^dM₂₈₂ T cells to help define properties that should be targeted by vaccines designed to elicit immunity mediated by CD8 T cells.

Results

RSV-specific CD8 T cell responses have epitope-dependent expansion capacity

Following RSV infection, expanded D^bM₁₈₇ and K^dM₂₈₂ T cells were quantified by fluorochrome-conjugated epitope peptide-MHC class I complexes (pMHCs) with flow cytometry (S1 Fig). We previously reported that D^bM₁₈₇ and K^dM₂₈₂ T cells assumed a numerical hierarchy in lung [17], the primary site of RSV infection. Here, we show a similar hierarchy in spleen at relatively low magnitude (Fig 1A, $p < 0.001$ and $p = 0.001$, D^bM₁₈₇ and K^dM₂₈₂ T cells respectively). Using a well-developed *in vivo* labeling procedure to distinguish cells in lung parenchyma from those in vasculature [21, 22], we found both D^bM₁₈₇ and K^dM₂₈₂ T cells preferentially infiltrated into lung tissue (Fig 1B). Since these two subsets have similar precursor frequency in naïve mice and similar infiltrating capacity into the inflammatory site, there are other factors that determine the hierarchy [23]. The Ki-67 expression showed that K^dM₂₈₂ T cells were more proliferative than D^bM₁₈₇ T cells (Fig 1C), consistent with the numerical dominance.

D^bM₁₈₇ T cells have superior cytolytic activity

To functionally evaluate D^bM₁₈₇ and K^dM₂₈₂ T cell cytotoxicity *in vivo*, we co-transferred M₁₈₇ or M₂₈₂ peptide-loaded naïve spleen cells as targets with OVA₂₅₇ peptide-loaded controls into RSV-infected and naïve recipients, and recovered the donor cells 3 hours later. The donor target and control cells were identified and distinguished by fluorochrome spectra and fluorescence intensity (S2 Fig). Recovery ratio of live targets to controls from the infected recipients was compared to recovery ratio from naïve recipients to calculate specific cytotoxicity [24]. We found that the bulk cytotoxic hierarchy correlated with overall numerical hierarchy, as more M₂₈₂ peptide-loaded targets were lysed in RSV-infected recipients than M₁₈₇ peptide-loaded targets (Fig 2A). Although lung had higher D^bM₁₈₇ and K^dM₂₈₂ T cell frequency and counts than spleen (Fig 1A and S3 Fig), there were more targets lysed in spleen than in lung ($p = 0.0047$ and $p = 0.0016$, M₁₈₇ and M₂₈₂ peptide-loaded respectively). The data suggest that cytotoxic potency may differ at the individual effector cell level.

To evaluate individual cell cytotoxicity, we divided lysed ratio of donor targets by frequency of endogenous CD8 T effector cells with relevant pMHC specificity, and expressed cytotoxic potency of individual effector cells in “killing” units. This value represents a relative frequency

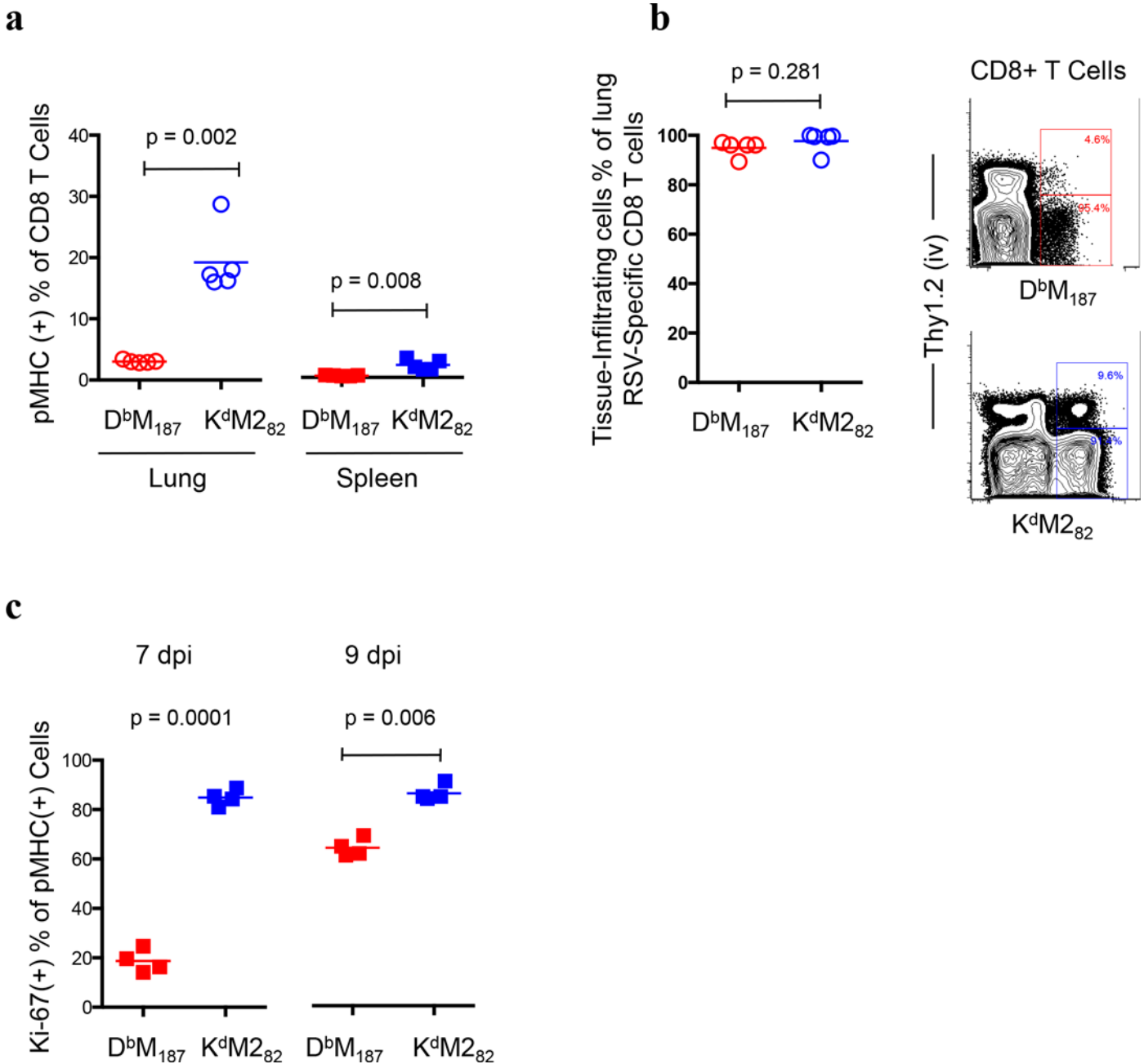


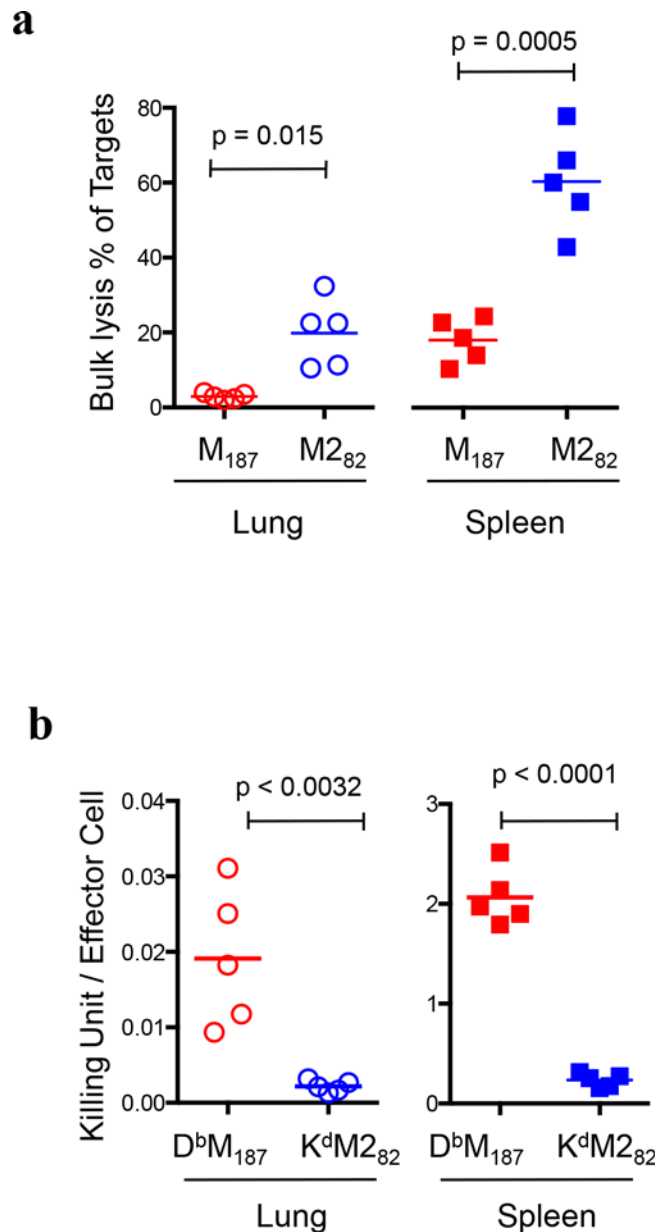
Fig 1. Numerical dominance of K^dM_{282} T cell response is associated with expansion capacity. (a) Magnitude of D^bM_{187} and K^dM_{282} T cell response at 7 dpi. Frequency of D^bM_{187} and K^dM_{282} T cells in CD8 T cell population were quantitatively assessed with flow cytometry. Data represent 5 independent experiments ($n = 5/\text{group}/\text{experiment}$). (b) The D^bM_{187} and K^dM_{282} T cells infiltrate into lung parenchyma following RSV infection. Lung lymphocytes were isolated from RSV- infected mice at 7 dpi. T cells in vasculature were pre-labeled by intravenous anti-Thy1.2 staining prior to euthanizing mice. Proportion of D^bM_{187} and K^dM_{282} T cells in lung parenchyma were quantitatively assessed with flow cytometry. Data represent 3 independent experiments ($n = 5/\text{group}/\text{experiment}$). (c) Lymphocytes isolated from spleens at 7 and 9 dpi were studied for Ki-67 expression by flow cytometry. The frequencies of Ki-67(+) cells in D^bM_{187} and K^dM_{282} T cell subsets are shown. Data represent 3 independent experiments ($n = 4/\text{group}/\text{experiment}$). All data are shown as mean with independent data point and compared by Student t-test. Each symbol represents one mouse.

doi:10.1371/journal.ppat.1005486.g001

of targets lysed by individual CD8 T effector cells. We found that individual D^bM_{187} T cells lysed more targets than K^dM_{282} T cells (Fig 2B), and both subsets more efficiently lysed targets in spleen than they did in lung ($p < 0.0001$ for both D^bM_{187} and K^dM_{282} T cells).

D^bM₁₈₇ T cells have high avidity TCR and enhanced effector-function signaling pathways

Since T cell cytotoxic potency has been associated with TCR avidity, we studied dissociation of pMHCs from cells as a surrogate measurement of TCR avidity. By measuring half-life ($T_{1/2}$) of maximum median fluorescence intensity (MFI), we found that D^bM₁₈₇ tetramers were retained



on CD8 T cells longer (59.62 and 405.7 min., lung and spleen respectively) than K^dM2_{82} tetramers (25.07 and 28.51 min., lung and spleen respectively) (Fig 3A). The dissociation rate (k) was calculated using Equation of Dissociation Kinetics in Prism 6 (Version 6.0f), and demonstrated that D^bM_{187} tetramer fell off CD8 T cells at lower rates (0.012 and 0.002, lung and spleen respectively) than K^dM2_{82} tetramer (0.028 and 0.024, lung and spleen respectively). The data suggest that TCRs recognizing D^bM_{187} have higher avidity than those recognizing K^dM2_{82} , and that avidity correlates with the individual cell cytotoxic potency. In addition, the data also indicate that CD8 T cells in spleen have higher TCR avidity than those in lung, suggesting that the binding capacity may be diminished in the setting of high antigen load and high level of T cell activation, or TCR may be down regulated.

Since TCR expression levels may have an effect on the expansion of antigen-specific cells, we assessed expression of TCR V β on CD8 T cells and found that K^dM2_{82} T cells have slightly higher level of TCR expression than D^bM_{187} T cells in lung, but not in spleen (S4 Fig). This difference may provide a partial explanation for the numerical hierarchy.

Transcriptional profiling of 8365 immune response-related genes revealed a distinct pattern in D^bM_{187} and K^dM2_{82} T cells (S5A Fig). Among the top 25 up-regulated genes in each subset, genes related to cytotoxic function and effector-memory differentiation (eg. *H2*, *cd40*, and *ccr6*) were up-regulated in D^bM_{187} T cells, while genes related to cell division (eg. *cdk2* and *cdc6*) were up-regulated in K^dM2_{82} T cells (S5B Fig). Analyzing those with fold change (FC) \geq Log₂1.3, $p < 0.05$ and FDR < 0.25 , the up-regulated gene sets in D^bM_{187} T cells were related to effector-function pathways, such as cytotoxicity, cytokine and chemokine production, memory differentiation, co-stimulatory signaling and cell survival signaling, while those in K^dM2_{82} T cells were related to promoting cell cycle and clonal expansion (Fig 3B). The expression of genes encoding cell-division cycle proteins, cell division cycle-associated proteins, mini-chromosome maintenance proteins, histones and cyclin-dependent kinases (S5C Fig) is consistent with post-transcriptional expression of Ki-67, which supports the findings that numerical hierarchy is associated with proliferative capacity.

D^bM_{187} T cells express an effector- and central-memory phenotype

Comparing gene expressions related to cell differentiation, D^bM_{187} T cells had elevated expression of *bcl6*, *ccr6*, *ccr7*, *il7r*, *fos*, *myc*, *sell* and *tcf7* (Fig 4A) that have been associated with effector-memory differentiation [25, 26]. In contrast, K^dM2_{82} T cells had elevated expression of *eomes*, *id-2*, *klrg-1*, *roar* and *tbx21*, factors associated with terminal differentiation [25, 27, 28]. Phenotyping by flow cytometry confirmed the transcriptional profiles, in that more than 50% of D^bM_{187} T cells were CD62L(-) and CD127(+), a phenotype of effector memory, compared to 37% of K^dM2_{82} T cells in lung, and 23% of D^bM_{187} T cells were CD62L(+) and CD127(+), a phenotype of central-memory, in spleen, while only 9% of K^dM2_{82} T cells expressed both memory markers (Fig 4B and S6A Fig). We assessed epitope-specific CD8 T cell populations and their phenotype at 8 weeks post RSV infection. Our data showed that D^bM_{187} T cells have a higher frequency of cells with central memory phenotype (CD62L+ & CD127+) than K^dM2_{82} T cells, and the central memory cell counts are the same although K^dM2_{82} T cell have a greater total cell count denominator than D^bM_{187} T cells at peak of response (S6b Fig). These data provide additional evidence that D^bM_{187} T cells are more likely to differentiate towards a central memory phenotype and survive after virus clearance.

Activated K^dM2_{82} T cells are susceptible to inhibitory regulation and apoptosis

T cell function is regulated by inhibitory receptors. Transcriptional profiling revealed that K^dM2_{82} T cells up-regulated expression of multiple inhibitory receptor genes (Fig 5A), such as

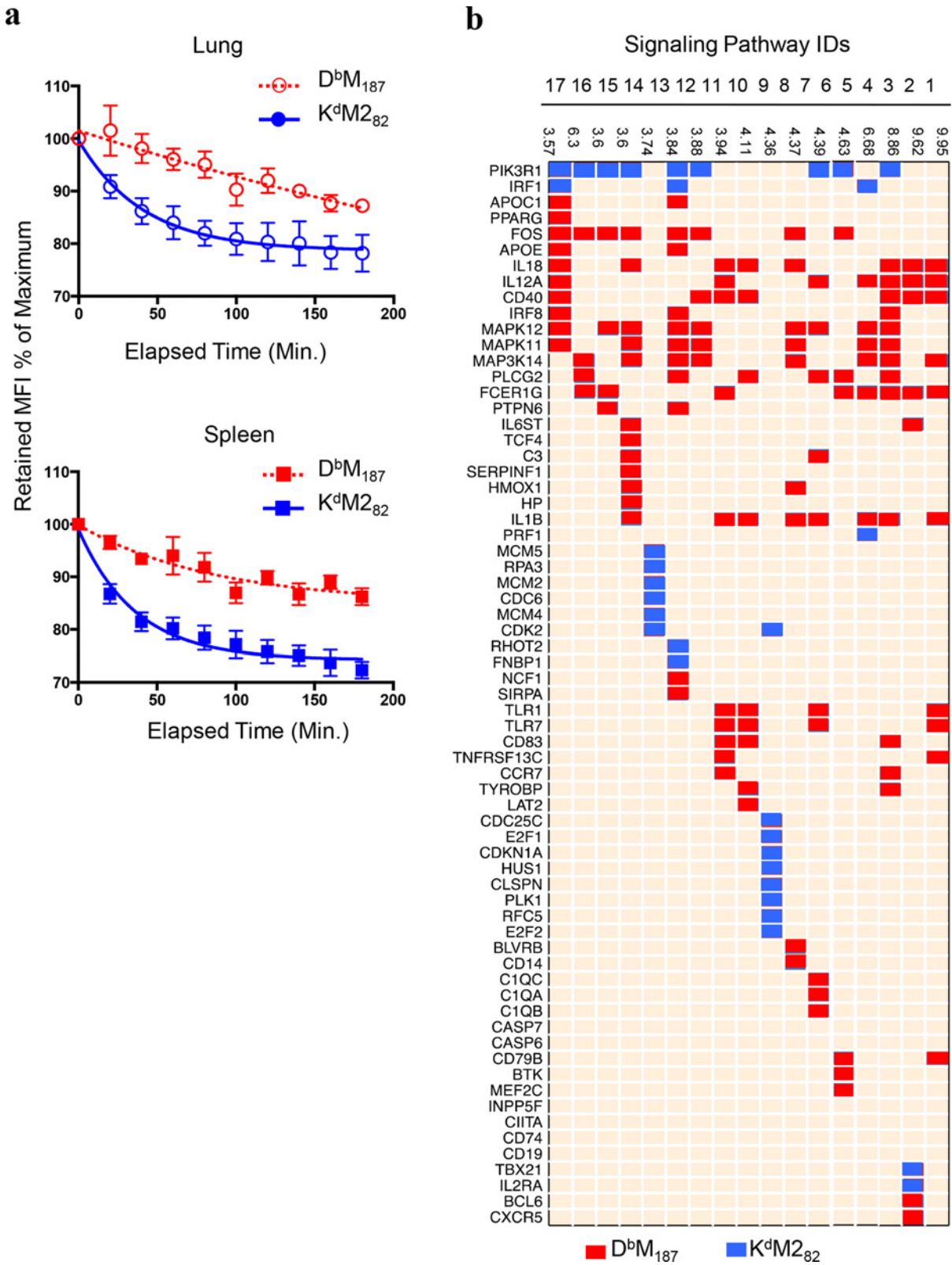


Fig 3. The D^bM_{187} T cells express high avidity TCR and signaling pathways promoting cytotoxic function. (a) The TCR avidity was assessed by dissociation of D^bM_{187} and K^dM_{282} from CD8 T cells. CD8 T cells were labeled with pMHCs and assessed cell-bound median fluorescence intensity (MFI) at indicated time point by flow cytometry. The MFI at 0 min was defined as the maximum measurement (100%). Data were analyzed with one-phase

exponential decay using nonlinear regression, and shown at mean \pm SEM of three independent experiments ($n = 5$ /group/experiment). **(b)** Transcriptional expression of genes that are up-regulated after RSV infection and associated with conventional signaling pathways. The D^bM_{187} , K^dM_{282} , and bulk CD8 T cells were sorted from spleen lymphocytes by FACS at 7 dpi. The mRNAs were isolated, amplified and labeled, then hybridized onto Illumina Mouse Chips. The quantitative gene expression were analyzed and normalized. Genes with Log_2 Fold Change (FC) > 1.3 , $p < 0.05$ and $\text{FDR} < 0.25$ (listed on left side of the chart) and associated signaling pathways were shown (Pathways 1: Altered T Cell and B Cell Signaling in Rheumatoid Arthritis; 2: T Helper Cell Differentiation; 3: Dendritic Cell Maturation; 4: Type I Diabetes Mellitus Signaling; 5: Role of NFAT in Regulation of the Immune Response; 6: Role of Pattern Recognition Receptors in Recognition of Bacteria and Viruses; 7: IL-10 Signaling; 8: Role of CHK Proteins in Cell Cycle Checkpoint Control; 9: TREM1 Signaling; 10: Communication between Innate and Adaptive Immune Cells; 11: CD40 Signaling; 12: Production of Nitric Oxide and Reactive Oxygen Species in Macrophages; 13: Cell Cycle Control of Chromosomal Replication; 14: Acute Phase Response Signaling; 15: CD28 Signaling in T Helper Cells; 16: PKC Signaling in T Lymphocytes; 17: IL-12 Signaling and Production in Macrophages.). Data were pooled from 10 or 11 individual mice in each group.

doi:10.1371/journal.ppat.1005486.g003

cd160, *cd223*, *cd152*, *ctla-4* and *sosc2*[29]. This is consistent with our phenotype study that showed PD-1, CD160 and CD223 expression was more common on K^dM_{282} T cells than on D^bM_{187} T cells (Fig 5B). Although D^bM_{187} T cells elevated *cd272* (*btla*) expression, another inhibitory receptor gene, the post-transcription level was similar to that of K^dM_{282} T cells (S7A

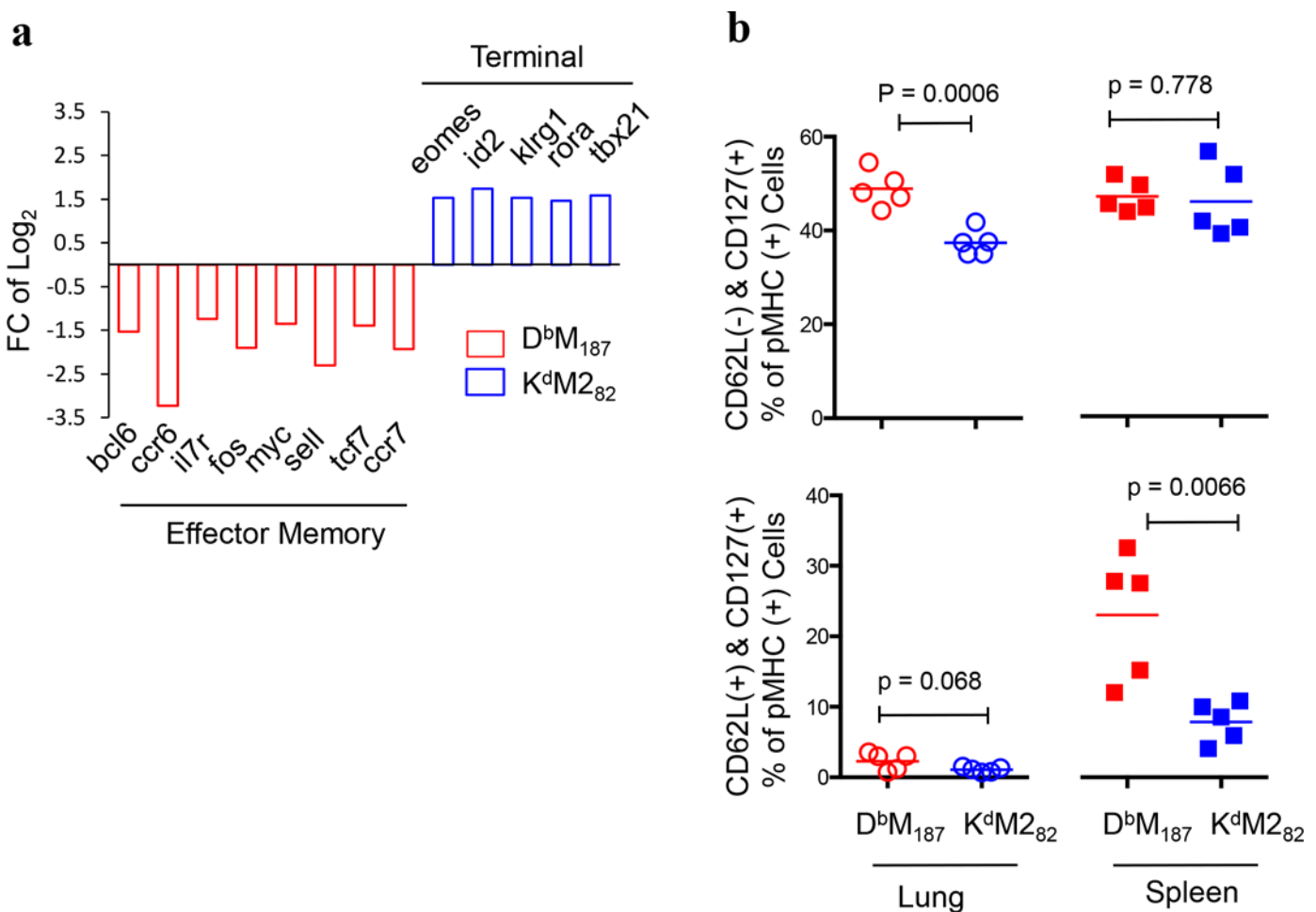


Fig 4. The D^bM_{187} T cells differentiate toward to an effector- and central-memory phenotype. **(a)** Transcriptional expressions that are associated with cell differentiation were analyzed and normalized. Relative expression was calculated and presented as Log_2 Fold Change (Log_2FC). The $\text{Log}_2\text{FC} = \text{Log}_2 K^dM_{282} - \text{Log}_2 D^bM_{187}$. Positive values indicate a specific gene expression was up-regulated in the K^dM_{282} subset, while negative values indicate up-regulated gene expression in the D^bM_{187} subset. Genes with expression differences of $\text{FC} > 1.3$, $p < 0.05$ and $\text{FDR} < 0.25$ are listed. Data were pooled from 10 or 11 individual mice in each group. **(b)** Post-transcriptional expression of CD62L and CD127. The CD62L(-)CD127(+) and CD62L(+)CD127(+) frequencies at 7 dpi were assessed by flow cytometry and are shown as mean with independent data point and compared by Student's *t*-test. Data represent 5 independent experiments ($n = 5$ /group/experiment). Each symbol represents one mouse.

doi:10.1371/journal.ppat.1005486.g004

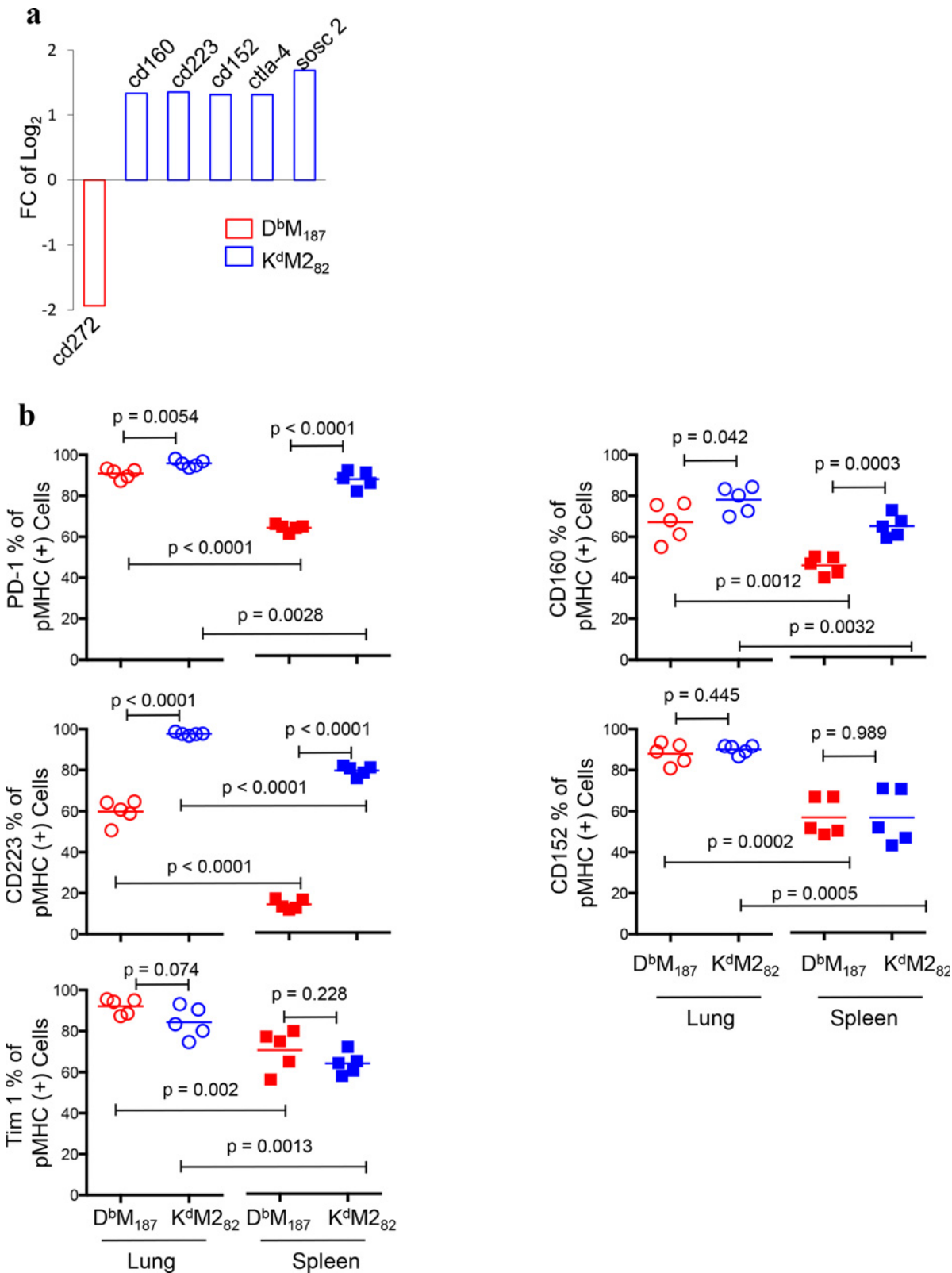


Fig 5. Activated K^dM₂₈₂ T cells up-regulate expression of inhibitory receptors. (a) Transcriptional expression of genes encoding inhibitory receptors with FC > ±1.3, p < 0.05 and FDR < 0.25 were listed. Data were pooled from 10 or 11 individual mice in each group. (b) Post-transcriptional expression of inhibitory receptors at 7 dpi was assessed by flow cytometry. The frequencies are shown as mean with independent data point and compared by Student's t-test. Data represent 5 independent experiments (n = 5/group/experiment). Each symbol represents one mouse.

doi:10.1371/journal.ppat.1005486.g005

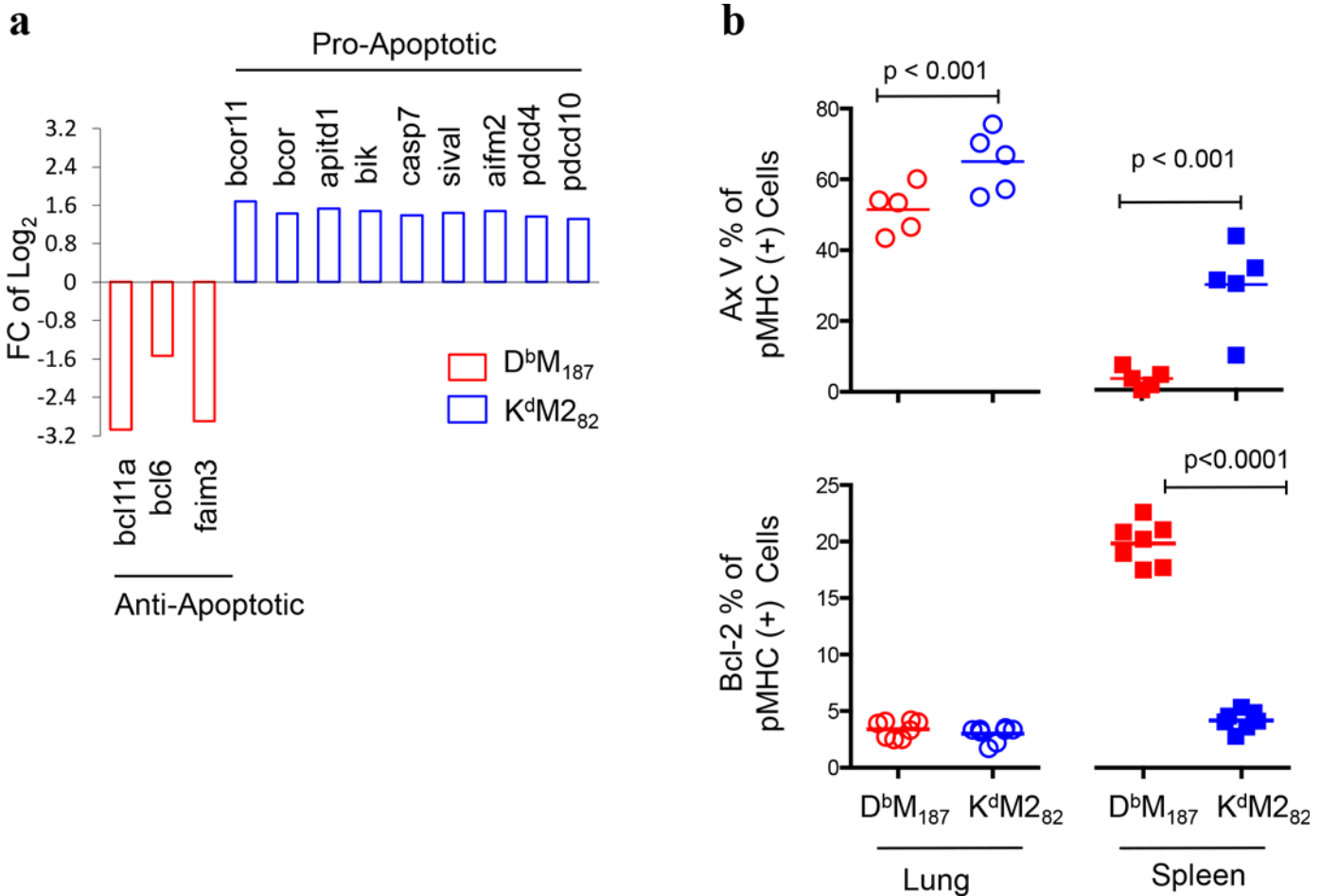


Fig 6. Activated K^dM₂₈₂ T cells are apoptotic. (a) Transcriptional expression of genes encoding pro- and anti-apoptosis molecules with FC > ±1.3, p < 0.05 and FDR < 0.25 were listed. Data were pooled from 10 or 11 individual mice in each group. (b) Apoptotic cells were identified by Annexin V staining, and post-transcriptional expression of Bcl-2 was identified by monoclonal antibody with flow cytometry at 7 dpi. The frequencies are shown as mean with independent data point and compared by Student's *t*-test. Data represent 3 or 4 independent experiments (n = 5/group/experiment). Each symbol represents one mouse.

doi:10.1371/journal.ppat.1005486.g006

Fig. We also found that cells isolated from lung were more likely to express inhibitory receptors than those isolated from spleen, including CD152, Tim1 and Tim3, although the difference in Tim3 expression was not statistically significant (**S7B Fig**). The transcriptional profile and phenotype of inhibitory receptors inversely correlate with individual D^bM₁₈₇ and K^dM₂₈₂ T cell cytotoxic potency and suggest that the K^dM₂₈₂ T cells are more susceptible to inhibitory regulation than the D^bM₁₈₇ T cells.

TCR ligation triggers activation-induced cell death that also negatively regulates T cell function. The expression of pro-apoptotic genes, such as *bcor*, *bcor11*, *apitd1*, *bik*, *casp7*, *sival*, *aimf2*, *pdcd4* and *pdcd10* [30–38], were up-regulated in K^dM₂₈₂ T cells, while those associated with anti-apoptosis, such as *bcl11a*, *bcl6* and *faim3* [39–41], were up-regulated in D^bM₁₈₇ T cells (**Fig 6A**). The *bcl11a* was also one of the top 25 up-regulated genes in D^bM₁₈₇ T cells (**S5B Fig**). Flow cytometry analysis showed that K^dM₂₈₂ T cells were more likely to be stained with Annexin V than D^bM₁₈₇ T cells, which is an early indication of apoptotic change (**Fig 6B**). In contrast, D^bM₁₈₇ T cells were more likely to express Bcl-2 than K^dM₂₈₂ T cells. Both CD8 T cell subsets from lung were more apoptotic than those from spleen (p < 0.0001, D^bM₁₈₇ and K^dM₂₈₂ T cells). The pattern of pro- and anti-apoptotic molecule expression at both

transcriptional and protein levels suggests that a large proportion of the CD8 T cells, particularly K^dM2_{82} T cells, progress towards apoptosis at the site of inflammation.

D^bM_{187} T cells efficiently control viral replication with limited pulmonary inflammation and disease severity

To evaluate capacity of controlling virus replication *in vivo*, we sorted live D^bM_{187} , K^dM2_{82} , and bulk (with neither specificity) CD8 T cells by FACS from the spleen of RSV-infected mice and transferred equal numbers into naive recipients. The recipients were then challenged with RSV one day later. At 4 days post infection (4 dpi), we detected $0.9 \pm 0.3\%$ D^bM_{187} and $0.8 \pm 0.5\%$ K^dM2_{82} T cells (mean \pm SD) in recipient's lung CD8 T cell population respectively. The epitope-specific CD8 T cells were not detectable above background ($\leq 0.05\%$ of CD8 T cells) in mice that received bulk CD8 T cells or CD8 T cells with irrelevant pMHC specificity (Fig 7A). This indicates that virtually all the epitope-specific CD8 T effector cells in lung at 4 dpi are donor origin. This is consistent with previous studies that have shown endogenous RSV-specific CD8 T cells are rarely detectable at 4 dpi of primary infection. Assessing anti-viral activity of isolated lung samples *in vitro*, we found that D^bM_{187} T cell recipients had significantly less viral replication in lungs than K^dM2_{82} or bulk CD8 T cell recipients (Fig 7B). K^dM2_{82} T cell recipients had similar viral replication in lungs as bulk CD8 T cell recipients ($p = 0.115$). We assessed IFN- γ in lung tissue homogenates, and found no significant difference among the recipient groups (S8 Fig). Although D^bM_{187} T cells have more efficient effector cytokine production at the individual cell level than K^dM2_{82} T cells, the impact of cytokines from adoptively transferred donor cells is likely to be masked by high levels of endogenous cytokine production.

Adoptively transferred donor cells increased recipient precursor frequency of relevant pMHC specificity and slightly altered the endogenous hierarchy at the day 7 peak response (S9 Fig). D^bM_{187} T cell recipients had a reduced disparity of CD8 T cell responses (K^dM2_{82} : $D^bM_{187} = 3:1$) compared to bulk CD8 T cell recipients (K^dM2_{82} : $D^bM_{187} = 5:1$), while the K^dM2_{82} T cell recipients had exaggerated disparity (K^dM2_{82} : $D^bM_{187} = 10:1$). Histopathological evaluation of lung tissue revealed D^bM_{187} T cell recipients had decreased frequency and count of total T and CD8 T cells compared to bulk CD8 and K^dM2_{82} T cell recipients (Fig 8A). The K^dM2_{82} T cell recipients had similar T and CD8 T cell frequencies and total cell counts in lung compared to the bulk CD8 T cell recipients. There was no significant difference in CD4 T cell counts between groups (S10 Fig). Paraffin-embedded sections of formalin-inflated lungs at 7 dpi were stained with hematoxylin-eosin and evaluated by an independent pathologist in a blinded manner. Typically, pathology after primary infection is most severe between 8 and 10 dpi. The histopathology was analyzed on 7 dpi because the transfer of immune competent cells accelerated the time course of response. Mice without RSV infection had few infiltrates with few mononuclear cells present in the interstitium (S11 Fig). After RSV infection, lung shows inflammatory histology. Although the lung pathology of recipient groups did not show significant difference by an over-all pathology score, 13.85 ± 1.10 , 12.28 ± 0.79 and 15.43 ± 1.21 for D^bM_{187} , K^dM2_{82} T cell and bulk CD8 T cell recipients, respectively (mean \pm SD in a 1–15 scale level), the K^dM2_{82} T cell and bulk CD8 T cell recipients showed more peribronchiolar neutrophil infiltration and higher magnitude interstitial inflammation and macrophage infiltration, suggesting a greater non-specific inflammatory response compared to D^bM_{187} T cell recipients. Bulk CD8 T cell recipients had an intermediate phenotype with interstitial infiltrates composed of both mononuclear cells and polymorphonuclear leukocytes (PMNs), but without frank alveolitis (Fig 8B). Recipients of the immunodominant K^dM2_{82} T cells had hemorrhagic alveolitis characterized by inflammatory cells and red blood cells (RBCs) frequently found in the

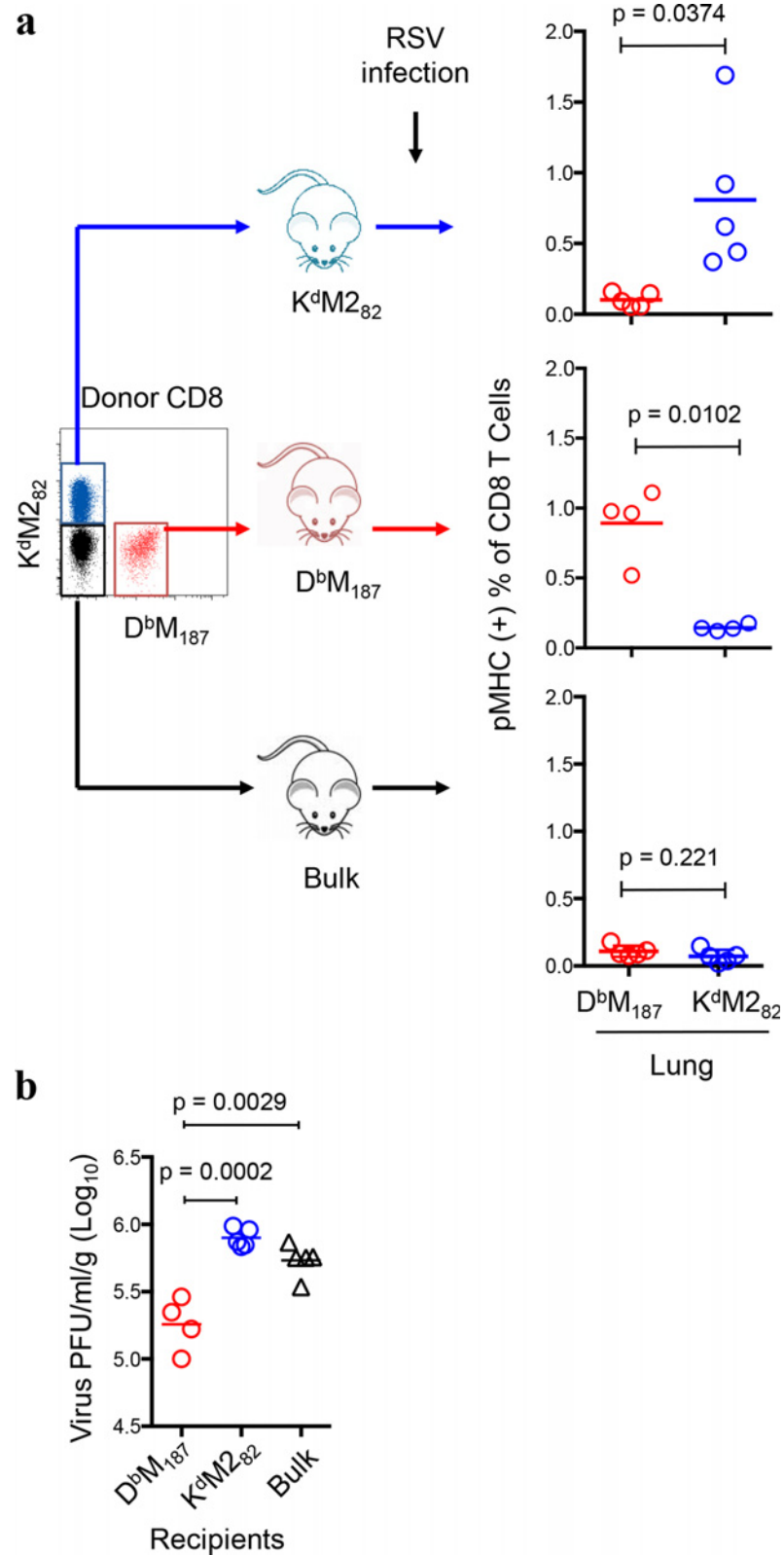


Fig 7. The D^bM_{187} T cells efficiently control viral replication. (a) Adoptive transfer of pMHC-specific donor cells increases precursor of CD8 T effector cells during early infection. Live D^bM_{187} , K^dM2_{82} and bulk (with neither specificity) CD8 T cells from spleen lymphocytes of RSV-infected mice at 7dpi were sorted with

FACS, and transferred into naive recipients respectively. The recipients were then challenged with RSV next day, and were evaluated for the donor D^bM₁₈₇ and K^dM₂₈₂ T cell frequencies in the right lung at 4 dpi by flow cytometry. **(b)** Viral activity in RSV challenged recipients. Left lungs of the RSV-challenged recipients were assessed for virus replication. The virus titers are expressed as log₁₀ PFU/gram of lung tissue. Data are shown as mean with independent data point and compared by Student's *t*-test. Data represent 3 independent experiments (n = 4 or 5/group/experiment). Each symbol represents one mouse.

doi:10.1371/journal.ppat.1005486.g007

alveolar space. The interstitial and alveolar infiltrates were composed primarily of mononuclear cells, but also contained a relative high frequency of PMNs. There was also evidence of epithelial necrosis with more pyknotic nuclei in this group. This is similar to the original report of CD8 transfer in H-2^d BALB/c mice causing hemorrhagic alveolitis[6]. The D^bM₁₈₇ T cell recipients had mononuclear cell interstitial infiltrates with rare PMNs and no cells in the alveolar space. This study indicates that the K^dM₂₈₂ T cells cause more tissue destruction and a more severe immunopathology than D^bM₁₈₇ T cells. We also monitored body weight change after virus challenge as a surrogate for severity of illness. All mice lost weight after RSV infection. However, the K^dM₂₈₂ T cell recipients had earlier and greater weight loss than other two groups. The differences were statistically significant from 5 to 7 dpi (Fig 8C, *p* < 0.05–0.005). The virus clearance, pathology and weight loss data indicate that D^bM₁₈₇ T cell-mediated virus clearance is more efficient and less pathogenic than that mediated by K^dM₂₈₂ T cells.

Discussion

It has become increasingly evident that magnitude of CD8 T cell response does not necessarily correlate with the extent of protection from infectious pathogens, and that functional properties of T cells may be more predictive of infection outcome[11, 12, 42]. In addition, the analysis of polyclonal T cell responses in bulk masks the functional diversity of T cells responding to specific epitopes. Even within an epitope-specific response, there are clonotype-specific subsets, each with their own functional profiles that collectively determine the characteristics of the overall response[9, 10]. Defining the characteristics of CD8 T cells that can efficiently clear virus-infected cells with minimal immunopathology has obvious implications for developing interventions that provide T cell-mediated immunity.

In the CB6F1 hybrid mouse model of RSV infection, numerically dominant K^dM₂₈₂ T cell response account for the majority of bulk cytolytic activity. But individual K^dM₂₈₂ T cells are relatively deficient in effector functions, and only about half of them produce IFN γ , which is a key molecule in eliminating virus infected cells[17, 43, 44]. Dramatically increasing K^dM₂₈₂ T cells to control RSV replication results in elevated pulmonary inflammation and disease severity[17, 18]. Informed by an earlier finding that virus clearance could be accomplished in mice infected with virus containing a mutated M₂₈₂ T cell epitope[20], we evaluated numerically subdominant CD8 T cell responses and found that individual D^bM₁₈₇ T cells were more efficient at lysing infected cells and controlling virus replication. CD8 T effector cells pre-existing in mucosal tissue have been reported to eliminate infection at the point of initial virus replication[45]. Adoptive transfer of D^bM₁₈₇ T cells increased pre-existing pulmonary CD8 T effector cells and controlled the virus replication during early infection. Prompt control of virus replication resulted in a mild infection-induced lung inflammation, with fewer infiltrating T cells, mononuclear cells and PMNs, and no hemorrhagic alveolitis or epithelial necrosis displayed in histological sections. As a consequence of the limited damage to lung tissue and function, the D^bM₁₈₇ T cell-mediated protection resulted in less illness than K^dM₂₈₂ T cell-mediated viral clearance. The efficiency of protection against virus challenge is an intrinsic property of D^bM₁₈₇ T cell cytolytic function, and is not associated with differences in migration, since K^dM₂₈₂ T cells have similar or higher presence in host lung[46].

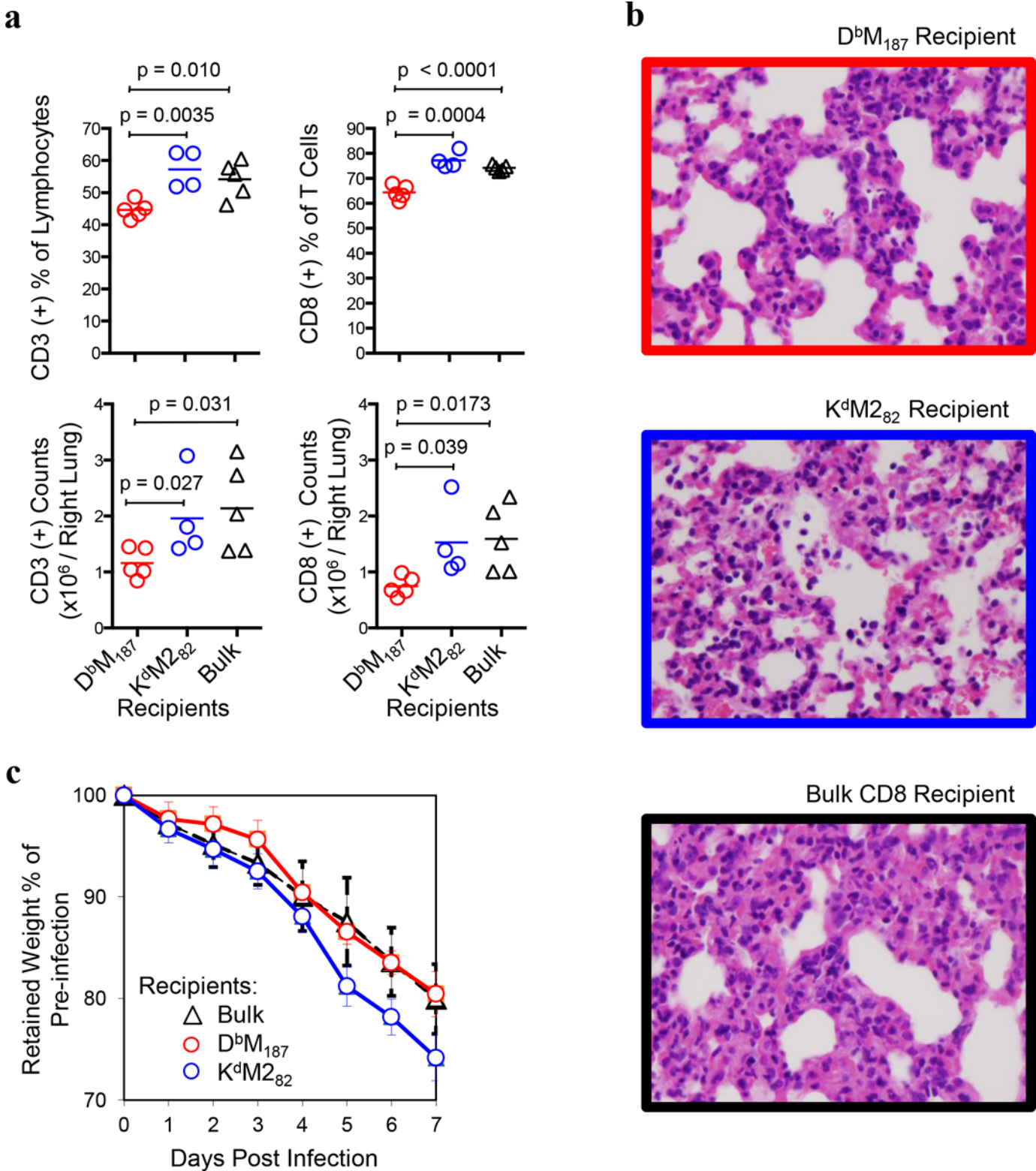


Fig 8. The D^bM₁₈₇ T cells provide protection with limited pulmonary inflammation and illness of the recipients. The D^bM₁₈₇, K^dM2₈₂ and bulk CD8 T cell recipients were challenged with RSV (a) Inflammatory cells were assessed at 7 dpi with flow cytometry. The absolute number and frequency of CD3 (+) cells and CD8 (+) T cells are expressed as mean with independent data point and are compared by Student's *t*-test. Data represent 3 independent experiments (*n* = 5/group/experiment). Each symbol represents one mouse. (b) Pathology of lung. Left lung of the virus-challenged recipients were studied

for histological change at 7 dpi. Microscopic study represents 3 independent experiments ($n = 5/\text{group/experiment}$). (c) Severity of illness. The virus-challenged recipients were weighed daily, from 0 to 7 dpi. Percentage represents retained proportion of pre-infection weight (mean \pm SEM). Data represent 3 independent experiments ($n = 5/\text{group/experiment}$) and are compared by Student *t*-test.

doi:10.1371/journal.ppat.1005486.g008

High TCR avidity has been suggested as a critical factor for induction of CD8 T cell effector function in viral infections[47, 48]. Our previous studies revealed that D^bM_{187} -specific TCRs recognize a more complex epitope structure and tend to have private clonotypes, presumably with a greater surface area of interaction with the epitope than K^dM_{282} -specific TCRs[49]. Here, our transcriptional profiling showed that the engagement of the high avidity D^bM_{187} -specific TCR activated pathways to promote effector function, survival, and effector-memory differentiation. The association of cytolytic potency with enhanced co-stimulation signaling, cytokine and chemokine production has been well studied and demonstrated to be a critical factor in anti-viral immunity[50]. The effector-memory phenotype is a subpopulation of CD8 T cells with particularly good functional activity. For example, CD8 T cells expressing an effector-memory phenotype were shown to be critical for protection from mucosal SIV challenge [51] and could clear virus-infected cells at an early stage of infection[52]. Our transcriptional, post-transcriptional, and long-term survival data suggest that D^bM_{187} -specific TCR engagement elicits a program driving cells toward effector-memory differentiation with higher cytotoxic potency than terminally differentiated cells driven by K^dM_{282} -specific TCR engagement.

Replication capacity accounts for the numerical dominance of K^dM_{282} T cell response. In some studies, precursors determine the magnitude of response[53, 54]. Our early study has showed that the frequency of D^bM_{187} and K^dM_{282} T cells are about the same in naïve mice[23]. Here, we showed that moderately increasing precursors of the subdominant subset by adoptive transfer influenced but did not reverse the hierarchy pattern. Difference in TCR level may provide partial explanation to the formation of numerical hierarchy but is not likely to be the major determinant. Recent studies reported that the level of TCR expression had minimal effect on the magnitude of antigen-specific CD8 T cells expansion[55, 56]. We also found that the differences in TCR expression levels were not proportional to differences in response magnitudes, and there is no significant difference in TCR expression levels on splenocytes. Variation in antigen dose may affect CD8 T cell expansion. But in our previous experiment using viral vector to express M and M2 antigens as a fusion protein, in which both epitopes were equally available and processed, we showed similar CD8 T cell response hierarchy as observed in RSV infection[23]. We propose that the extreme proliferation of K^dM_{282} T cells is presumably driven by activation signals derived from the pMHC-TCR interaction. K^dM_{282} T cells express TCRs that recognize a relatively flat and featureless epitope, and have a highly public clonotype[10]. These characteristics determine that K^dM_{282} T cells have distinct activation thresholds for proliferation and cytolytic activity or cytokine production. It has been reported that some epitope-specific CD8 T cells can be expanded by cognate peptide in the absence of helper cell-derived signals, although their effector functions might not be triggered[57]. Another study based on mathematic modeling concluded that rapid expanding T cells were likely to be deficient in effector function and short-lived[52]. It is possible that the rapidly dividing population has a diminished TCR avidity due to down-regulation. The type of exaggerated activation that leads to the numerical dominance of K^dM_{282} T cell response may be selected by immunogenicity testing based solely on magnitude of response, but is not the preferred adaptive immune response from the host perspective.

Our previous study reported that the K^dM_{282} T cells were selectively susceptible to regulatory CD4 T cells[20, 58]. Here, we showed that the K^dM_{282} T cells were subject to inhibitory signals, by elevated expression of PD-1, CD160, CD223 and other inhibitory receptors. These

inhibitory receptors have a negative impact on T cell effector function and control of viral replications in chronic[29] and acute infections[59]. RSV infection has been reported to induce PD-L1 expression on bronchial epithelial cells, which resulted in an inhibition of CD8 T cell antiviral activity[60]. The PD-1 and other inhibitory signals can also suppressed memory formation and directed CD8 T cells to terminal differentiation[29]. Being apoptotic has been shown to negatively impact effector function. The extremely activated and robustly proliferating K^dM2_{82} T cells up-regulate genes promoting apoptosis, but have reduced expression of genes encoding anti-apoptotic molecules. The inhibitory receptor expression and pro-apoptotic changes are consistent with the functional deficiency of K^dM2_{82} T cells, and with previous observations that only a fraction of the K^dM2_{82} T cells produce IFN- γ , while almost all D^bM_{187} T cells are IFN- γ -producing[17, 44].

The tissue environment may also have impact on CD8 T cell effector function. Terminal differentiation and lack of cytolytic capacity have been previously demonstrated to be a characteristic of lung-derived CD8 T cells in response to viral infections[57]. Terminally differentiated CD8 T cells in the lung had limited cytolytic activity and were unable to control influenza and Sendai virus infection[61]. Here, we found that D^bM_{187} and K^dM2_{82} T cells isolated from lung, where they are needed to clear virus-infected cells, were less cytotoxic than cells isolated from spleen. Our data suggest that cells in the lung are vulnerable to suppressive regulation by elevating expression of inhibitory receptors, and susceptible to activation-induced cell death by down-regulating anti-apoptotic molecules. Terminal differentiation and loss of effector function has been associated with prolonged TCR ligation and inflammatory cytokine-driven differentiation[62–64]. Persistent engagement of TCR can trigger down-regulation of CD127 on CD8 T cells in lung[65], and adversely affect control of viral replication[66]. Thus, a balanced and modulated inflammatory response promotes optimal CD8 T effector function.

In the mouse model of RSV infection, a subdominant CD8 T cell response provided adequate control of viral replication during early infection, limited the viral replication, and reduced pulmonary inflammation and disease severity. These data support the concept that induction of T cells with high cytolytic activity are more favorable for protecting the host from viral infection than a high magnitude response with cells exhibiting a more extreme differentiation phenotype. The goal for vaccine-induced CD8 T cell-mediated protection should be to increase the precursor frequency of cells that can respond rapidly based on a pre-existing memory phenotype and localization. They should exhibit potent and efficient cytolytic activity without excessive proliferation that may lead to unwarranted immunopathology[12]. These findings raise the interesting possibility that by selecting for T cell epitopes with more complex structures, it may be possible to elicit T cell responses that have higher TCR-pMHC avidity. These cells would be more likely to achieve the activation threshold for initiating the effector functions needed to rapidly clear virus-infected cells with minimal immunopathology.

Materials and Methods

Mice and virus infection

Pathogen-free CB6F1 female mice between the ages of 8 and 10 weeks were purchased from Jackson Laboratories (Bar Harbor, ME) and cared for in accordance with the NIH Guide for the Care and Use of Laboratory Animals. The NIH Animal Care and Use Committee approved all animal protocols in this study. Experimental groups were age matched. RSV challenge stock was derived from the A2 strain by sonicating HEP-2 cell monolayers as previously described [16]. For infection, mice were inoculated with 1×10^7 PFU live RSV in 10% EMEM intranasally under anesthesia with 3% isoflurane and oxygen.

Ethics statement

Animal use and all procedures (VRC-13-443 and -447) were approved by the Vaccine Research Center, Animal Care and Use Committee (ACUC) in accordance with NIH policy and ARAC guidelines, and is accredited by the Association for Assessment and Accreditation of Laboratory Animal Care (AAALAC) and in compliance with the Animal Welfare Act and Public Health Service Policy on Humane Care and Use of Laboratory Animals. The National Institutes of Health Intramural Research Program OLAW assurance number is A4149-01.

Cell culture and flow cytometry reagents

The cell culture medium was RPMI 1640 from HyClone (Logan, UT), supplemented with 10% heat inactivated fetal bovine serum, 2 mM glutamine, 10 U/ml penicillin and 10 µg/ml streptomycin. Fluorochrome-conjugated antibodies used to study cell phenotype, differentiation and other expressions with flow cytometry were anti-CD3–cyanine 7 (Cy7) allophycocyanin (APC), anti-Ki67–fluorescein isothiocyanate (FITC), anti-Bcl2–FITC, and Annexin V–FITC that were purchased from BD Biosciences (San Jose, CA). Unconjugated antibodies to CD4, CD8 and CD62L were purchased from Harlan (Indianapolis, IN) and were conjugated with Qdot605, Qdot655 and Alexa Fluor 688 from Invitrogen (Carlsbad, CA). The in-house conjugates were validated by comparison with commercial conjugates. Anti-PD-1–FITC, anti-CD272–phycoerythrin (PE), anti-CD152–PE, anti-Tim1–biotin, anti-Tim3–biotin, anti-CD223–PE and anti-CD127–Cy7PE were purchased from eBioscience Inc (San Diego, CA). Streptavidin (SA)–PE was purchased from ProZyme (Hayward, CA). Violet fluorescent reactive dye (Invitrogen, CA), anti-CD19- and anti-CD16/32–Pacific blue (eBioscience) were used as cell viability and lineage markers to exclude dead and non-T cells from analysis. Fluorochrome-conjugated epitope peptide–MHC class I complexes (pMHC), D^b–M₁₈₇₋₁₉₅–APC (D^bM₁₈₇–APC) and K^d–M₂₈₂₋₉₀–PE (K^dM₂₈₂–PE), were purchased from Beckman Coulter (Fulerton, CA).

In vivo T cell labeling

Naïve or RSV-infected mice were injected intravenously with Cy5PE-conjugated anti-Thy1.2 antibody purchased from BioLegend (San Diego, CA). Mice were sacrificed 10 min. later. Lymphocytes from lung and spleen were isolated and stained for lineage differentiation and pMHC specificity following standard procedures, and then applied to flow cytometry analysis[21, 22].

Cytotoxic activity assays

To evaluate cytotoxicity of D^bM₁₈₇ and K^dM₂₈₂ T cells *in vivo*, we setup an assay based on previous described[24]. The targets were prepared from naïve spleen cells that were loaded with M₁₈₇₋₁₉₅ (M₁₈₇) or M₂₈₂₋₉₅ (M₂₈₂) peptides (Anaspec Inc, San Jose, CA) at a concentration of 10 µg/ml, then stained with 10 uM carboxyfluorescein succinimidyl ester (CFSE) or 10 uM CellTracker Red CMTPX (both from Invitrogen) respectively; controls were prepared from naïve spleen cells that were loaded with OVA₂₅₇₋₂₆₄ (OVA₂₅₇) peptide (Anaspec Inc) at a concentration of 10 µg/ml, then stained with either 0.1 uM CFSE or 0.2 uM CellTracker Red CMTPX respectively. These four populations, including M₁₈₇–CFSE^{high}, M₂₈₂–CMTPX^{high}, OVA₂₅₇–CFSE^{low} and OVA₂₅₇–CMTPX^{low}, each at 2 x 10⁶, were co-transferred into RSV-infected or naïve mice via tail vein. Cells from the lung and spleen were collected 3 hours later from the recipients. Donor cells were identified by fluorochromes spectra and distinguished by fluorescence intensity. The specific lysis were calculated using formula: ratio = (percentage fluorochrome^{low}/percentage fluorochrome^{high}). Specific lysis (%) = [1 – (ratio naïve/ratio

infected) $\times 100$]. Frequency of pMHC-specific CD8 T cells was assessed simultaneously in the same cell preparation recovered. The cytolytic unit per pMHC specific CD8 T effector cell was calculated by dividing the percent of specific lysis by the frequency of pMHC-specific CD8 T cells.

TCR avidity assessment

The pMHC decay assessment was performed as described previously[67]. Briefly, lung and spleen lymphocytes from RSV-infected mice were stained for lineage differentiation and epitope specificity with fluorochrome-conjugated pMHCs. Cells were washed and then incubated in the presence of anti-H2-D^b (12.5 $\mu\text{g}/\text{ml}$) or anti-H2-K^d (2.5 $\mu\text{g}/\text{ml}$) respectively, in culture medium containing 0.1% sodium azide at room temperature. Cells were recovered every 20 minutes, washed and then fixed with 1% paraformaldehyde and applied for flow cytometry to assess the intensity of fluorescence.

Sorting and adoptive transfer of pMHC-specific donor cells

Live D^bM₁₈₇, K^dM₂₈₂ and bulk (with neither specificity) CD8 T cells from spleen lymphocytes of RSV-infected mice at 7dpi were sorted by FACS. From each population, 5×10^5 cells were transferred into naive recipients respectively via tail vein. The recipients were challenged with RSV 24 hours later, and were evaluated for the donor cell frequencies and the virus load.

Viral load assessment

Lung tissue was sampled at indicated times after RSV infection and quickly frozen using ethanol-dry ice in 10% EMEM medium. After grinding and pelleting of tissue debris, serial dilutions of supernatant were inoculated onto 80% confluent HEp-2 cell monolayers in triplicate and overlaid with 0.75% methylcellulose in 10% EMEM. The cultures were incubated at 37°C for 4 days, then fixed with phosphate buffered 10% formalin and stained with hematoxylin and eosin. Plaques were counted and expressed as \log_{10} PFU/gram of lung. The limit of detection is $1.8 \log_{10}$ PFU/gram of lung.

Histology

At indicated time points after RSV infection, mice were euthanized and the left lung was gently inflated with phosphate-buffered 10% formalin, then removed and placed in the buffered formalin. Thin sections were cut from paraffin-embedded lung tissues, stained with hematoxylin and eosin and examined by light microscopy.

Microarray cDNA hybridization analysis

Splenocytes from RSV-infected mice were isolated and stained for lineage differentiation and pMHC specificities. D^bM₁₈₇ and K^dM₂₈₂ T cells were sorted into RLT buffer (Qiagen, CA) with cell sorter Aria (BD Biosciences, CA). After isolation of mRNA, the total RNA was amplified and labeled using the Illumina TotalPrep RNA Amplification kit. The biotinylated cRNA was hybridized onto Illumina Mouse Chips and quantified using Illumina BeadStation 500GX scanner and Illumina BeadStudio v3 program. Illumina probe data were exported from BeadStudio as raw data and screened for quality. Samples failing chip visual inspection and control examination were removed. Gene expression data were analyzed using Bioconductor, an open-source software library for the analyses of genomic database on R, which is a language and environment for statistical computing and graphics (www.r-project.org). The R software package was used to first filter out probes with intensities below background in all samples, and

then to replace minimum (a surrogate replacement policy) values below background using the mean background value of the built-in Illumina probe controls as an alternative to background subtraction (which may introduce negative values) to reduce “overinflated” expression ratios determined in subsequent steps, and finally quantitatively normalize the probe intensities. The resulting matrix showing probes as rows and samples as columns was \log_2 transformed and used as input for linear modeling using BioConductor Linear models for microarray analysis (LIMMA). The LIMMA package was used to identify differentially expressed genes (pFDR < 0.05).

Accession numbers

Genes and proteins mentioned in the text can be found in the SwissProt data libraries (<http://www.uniprot.org/uniprot/>) under the following accession numbers: RSV-M (P03419), RSV-M2 (P04545), Ki-67 (Q61769), CD62L (P18337), CD127 (P16872), IFN γ (P01580), PD-1 (Q02242), CD160 (O88875), CD223 (Q61790), CD152 (P09793), Tim 1 (Q5QNS5), Annexin V (P48036), Bcl-2 (P10417).

Supporting Information

S1 Fig. Identification of D^bM₁₈₇ and K^dM₂₈₂ T cells by flow cytometry. Lymphocytes isolated from the lung and spleen of RSV-infected mice at 7 dpi were stained for CD3, CD4 and CD8 lineage differentiation and pMHC-specificities. Dot plots represent strategies to identify D^bM₁₈₇ and K^dM₂₈₂ T cells, by sequentially gating on singlets, lymphocytes, CD3(+) Dump(-), CD8(+) CD4(-), and pMHC(+) populations. The Dump channel included Violet fluorescent reactive dye, fluorochrom-conjugated anti-CD16/32 and anti-CD19 to exclude dead cells, monocytes, B cells, and other non-T cells. Dot plots represent 5 independent experiments (n = 5/group/experiment).

(TIF)

S2 Fig. Quantitative assessment of peptide-loaded and fluorochrome-labeled targets and controls recovered from recipients in cytotoxicity assay *in vivo*. After adopting peptide-loaded and fluorochrome-labeled targets and controls, the recipient’s lung and spleen cells were isolated 3 hours later and analyzed by flow cytometry. The M₁₈₇ and M₂₈₂ peptide-loaded targets were identified by high intensity of CFSE and CMTPX respectively; the OVA₂₅₇ peptide-loaded controls were identified by lower intensity of CFSE and CMTPX and used as controls for the same fluorochrome-labeled targets respectively. Histograms show the proportion of cells with distinct fluorochrome labeling and intensity recovered from infected or naïve mice. Dot plots and histograms represent 5 independent experiments (n = 5/group/experiment).

(TIF)

S3 Fig. The D^bM₁₈₇ and K^dM₂₈₂ T cell counts in lung and spleen. The D^bM₁₈₇ and K^dM₂₈₂ T cells from lung and spleen of infected mice at 7 dpi were quantitatively assessed by flow cytometry. Cell counts were calculated based on total cell counts in the lung and spleen cell preparations and the frequency of individual subsets. Data are shown as mean with independent data point and are compared by Student’s *t*-test. Data represent 5 independent experiments (n = 5/group/experiment). Each symbol represents one mouse.

(TIF)

S4 Fig. TCR level of D^bM₁₈₇ and K^dM₂₈₂ T cells. Lymphocytes isolated from the lung and spleen of RSV-infected mice at 7 dpi were stained for CD3, CD4 and CD8 lineage differentiation and pMHC-specificities. The expression of TCR on epitope-specific CD8 T cells was

studied using fluorescence-conjugated anti-TCR V β (pan V β) monoclonal antibody, and the relative level of expression was measured by the medium fluorescence intensity (MFI). Data are shown as mean with independent data point and are compared by Student's *t*-test. Data represent 2 independent experiments ($n = 5$ /group/experiment). Each symbol represents one mouse.

(TIF)

S5 Fig. Pattern of Transcriptional expressions of D^bM₁₈₇ and K^dM₂₈₂ T cells. The D^bM₁₈₇, K^dM₂₈₂ and bulk CD8 T cells were sorted from spleen by FACS at 7 dpi and studied for transcriptional expression of genes associated to immune responses. The quantitative gene expression were analyzed and normalized. Relative expression was calculated and presented as Log₂ Fold Change (Log₂FC). The Log₂FC = Log₂ K^dM₂₈₂ - Log₂ D^bM₁₈₇. Positive values indicate gene expression was up-regulated in the K^dM₂₈₂ subset, while negative values indicate gene expression was up-regulated in the D^bM₁₈₇ subset. **(a)** All gene expressions with Log₂ FC > ± 1.3 . **(b)** Top 25 up-regulated expressions among (a) in each subset. **(c)** Up-regulated expressions of genes in (a) related to MHC class I molecule and clone expansion. Each column represents data from one mouse.

(TIF)

S6 Fig. Pattern of CD62L and CD127 expression and memory subsets. Lymphocytes were isolated from the lung and spleen of infected mice at 7dpi and studied for expression of CD62L and CD127 with flow cytometry. Dot plots show the gating strategy and represent 5 independent experiments ($n = 5$ /group/experiment). **(b)** Lymphocytes were isolated from the lung and spleen of mice at 8 weeks post infection. The D^bM₁₈₇ and K^dM₂₈₂ T cells were studied for their frequency, count, and expression of CD62L and CD127 with flow cytometry. Data are shown as individual data points with horizontal bar representing the mean, and are compared by Student's *t*-test. Data represent 2 independent experiments ($n = 5$ /group/experiment). Each symbol represents one mouse.

(TIF)

S7 Fig. Similar expression of CD272 and Tim 3 in D^bM₁₈₇ and K^dM₂₈₂ T cells. Lymphocytes were isolated from the lung and spleen of infected mice at 7dpi and studied for expression of **(a)** CD272 and **(b)** Tim 3 with flow cytometry. The frequencies are shown as mean with independent data point and compared by Student's *t*-test. Data represent 5 independent experiments ($n = 5$ /group/experiment). Each symbol represents one mouse.

(TIF)

S8 Fig. Lung IFN- γ level of recipients after RSV challenge. Lung supernatant described in [Fig 7B](#) were collected and frozen saved. INF- γ level was assessed using LEGENDplex (BioLegend), a bead-based commercially available immunoassay service. The concentration was calculated referring to standard series. Each symbol represents one mouse ($n = 11$).

(TIF)

S9 Fig. Adapting donor cells increases frequency of CD8 T cells with relevant specificity after virus challenge. After virus challenge, the recipients that adopted D^bM₁₈₇, K^dM₂₈₂ and bulk CD8 T cells were evaluated for D^bM₁₈₇ and K^dM₂₈₂ T cell frequencies in the right lung at 7 dpi with flow cytometry. The frequencies are shown as mean with independent data point and compared by Student's *t*-test. Data represent 3 independent experiments ($n = 4$ or 5 /group/experiment). Each symbol represents one mouse.

(TIF)

S10 Fig. CD4 T cell counts were not significantly altered in recipients. The D^bM₁₈₇, K^dM₂₈₂ and bulk CD8 T cell recipients were challenged with RSV. Inflammatory cells were assessed at 7 dpi with flow cytometry. The absolute number and frequency of CD4 (+) cells are expressed as mean with independent data point and are compared by Student's *t*-test. Data represent 3 independent experiments (n = 5/group/experiment). Each symbol represents one mouse. (TIF)

S11 Fig. Histology of naïve lung. Left lung were isolated from naïve mice and studied for the histology of lung structure. Sections were examined under light microscope by independent blinded investigators. Histology study represents 3 independent experiments (n = 5). (TIF)

Acknowledgments

We thank Flow Cytometry Core for cell sorting service, Animal Facility for taking care of experimental mice, and Dr. Tracy Ruckwardt for helpful comments.

Author Contributions

Conceived and designed the experiments: JL BSG. Performed the experiments: JL JM SSR KMM. Analyzed the data: JL EKH AFM RPS BSG KMM. Contributed reagents/materials/analysis tools: EKH RPS. Wrote the paper: JL BSG.

References

- Welliver TP, Garofalo RP, Hosakote Y, Hintz KH, Avendano L, Sanchez K, et al. Severe human lower respiratory tract illness caused by respiratory syncytial virus and influenza virus is characterized by the absence of pulmonary cytotoxic lymphocyte responses. *J Infect Dis.* 2007; 195(8):1126–36. Epub 2007/03/16. doi: JID37165 [pii] doi: [10.1086/512615](https://doi.org/10.1086/512615) PMID: [17357048](https://pubmed.ncbi.nlm.nih.gov/17357048/).
- Shah JN, Chemaly RF. Management of RSV infections in adult recipients of hematopoietic stem cell transplantation. *Blood.* 117(10):2755–63. Epub 2010/12/09. doi: blood-2010-08-263400 [pii] doi: [10.1182/blood-2010-08-263400](https://doi.org/10.1182/blood-2010-08-263400) PMID: [21139081](https://pubmed.ncbi.nlm.nih.gov/21139081/).
- Milstone AP, Brumble LM, Barnes J, Estes W, Loyd JE, Pierson RN 3rd, et al. A single-season prospective study of respiratory viral infections in lung transplant recipients. *Eur Respir J.* 2006; 28(1):131–7. Epub 2006/03/03. doi: 09031936.06.00105505 [pii] doi: [10.1183/09031936.06.00105505](https://doi.org/10.1183/09031936.06.00105505) PMID: [16510454](https://pubmed.ncbi.nlm.nih.gov/16510454/).
- Hall CB, Powell KR, MacDonald NE, Gala CL, Menegus ME, Suffin SC, et al. Respiratory syncytial viral infection in children with compromised immune function. *N Engl J Med.* 1986; 315(2):77–81. Epub 1986/07/10. doi: [10.1056/NEJM198607103150201](https://doi.org/10.1056/NEJM198607103150201) PMID: [3724802](https://pubmed.ncbi.nlm.nih.gov/3724802/).
- El Saleeby CM, Suzich J, Conley ME, DeVincenzo JP. Quantitative effects of palivizumab and donor-derived T cells on chronic respiratory syncytial virus infection, lung disease, and fusion glycoprotein amino acid sequences in a patient before and after bone marrow transplantation. *Clin Infect Dis.* 2004; 39(2):e17–20. Epub 2004/08/13. doi: [10.1086/421779](https://doi.org/10.1086/421779) CID32988 [pii]. PMID: [15307047](https://pubmed.ncbi.nlm.nih.gov/15307047/).
- Cannon MJ, Openshaw PJ, Askonas BA. Cytotoxic T cells clear virus but augment lung pathology in mice infected with respiratory syncytial virus. *J Exp Med.* 1988; 168(3):1163–8. Epub 1988/09/01. PMID: [3262705](https://pubmed.ncbi.nlm.nih.gov/3262705/); PubMed Central PMCID: PMC2189034.
- Graham BS, Bunton LA, Wright PF, Karzon DT. Role of T lymphocyte subsets in the pathogenesis of primary infection and rechallenge with respiratory syncytial virus in mice. *J Clin Invest.* 1991; 88(3):1026–33. Epub 1991/09/01. doi: [10.1172/JCI115362](https://doi.org/10.1172/JCI115362) PMID: [1909350](https://pubmed.ncbi.nlm.nih.gov/1909350/); PubMed Central PMCID: PMC295511.
- Tregoning JS, Yamaguchi Y, Harker J, Wang B, Openshaw PJ. The role of T cells in the enhancement of respiratory syncytial virus infection severity during adult reinfection of neonatally sensitized mice. *J Virol.* 2008; 82(8):4115–24. Epub 2008/02/15. doi: JVI.02313-07 [pii] doi: [10.1128/JVI.02313-07](https://doi.org/10.1128/JVI.02313-07) PMID: [18272579](https://pubmed.ncbi.nlm.nih.gov/18272579/); PubMed Central PMCID: PMC2293007.
- Newell EW, Sigal N, Bendall SC, Nolan GP, Davis MM. Cytometry by time-of-flight shows combinatorial cytokine expression and virus-specific cell niches within a continuum of CD8+ T cell phenotypes.

- Immunity. 2012; 36(1):142–52. doi: [10.1016/j.immuni.2012.01.002](https://doi.org/10.1016/j.immuni.2012.01.002) PMID: [22265676](https://pubmed.ncbi.nlm.nih.gov/22265676/); PubMed Central PMCID: [PMC3752833](https://pubmed.ncbi.nlm.nih.gov/PMC3752833/).
10. Billam P, Bonaparte KL, Liu J, Ruckwardt TJ, Chen M, Ryder AB, et al. T Cell receptor clonotype influences epitope hierarchy in the CD8+ T cell response to respiratory syncytial virus infection. *J Biol Chem*. 2011; 286(6):4829–41. doi: [10.1074/jbc.M110.191437](https://doi.org/10.1074/jbc.M110.191437) PMID: [21118816](https://pubmed.ncbi.nlm.nih.gov/21118816/); PubMed Central PMCID: [PMC3039322](https://pubmed.ncbi.nlm.nih.gov/PMC3039322/).
 11. Gallimore A, Dumrese T, Hengartner H, Zinkernagel RM, Rammensee HG. Protective immunity does not correlate with the hierarchy of virus-specific cytotoxic T cell responses to naturally processed peptides. *J Exp Med*. 1998; 187(10):1647–57. Epub 1998/06/13. PMID: [9584143](https://pubmed.ncbi.nlm.nih.gov/9584143/); PubMed Central PMCID: [PMC2212291](https://pubmed.ncbi.nlm.nih.gov/PMC2212291/).
 12. Frahm N, Kiepiela P, Adams S, Linde CH, Hewitt HS, Sango K, et al. Control of human immunodeficiency virus replication by cytotoxic T lymphocytes targeting subdominant epitopes. *Nat Immunol*. 2006; 7(2):173–8. Epub 2005/12/22. doi: [ni1281](https://doi.org/10.1038/ni1281) [pii] doi: [10.1038/ni1281](https://doi.org/10.1038/ni1281) PMID: [16369537](https://pubmed.ncbi.nlm.nih.gov/16369537/).
 13. Hansen SG, Sacha JB, Hughes CM, Ford JC, Burwitz BJ, Scholz I, et al. Cytomegalovirus vectors violate CD8+ T cell epitope recognition paradigms. *Science*. 2013; 340(6135):1237874. doi: [10.1126/science.1237874](https://doi.org/10.1126/science.1237874) PMID: [23704576](https://pubmed.ncbi.nlm.nih.gov/23704576/).
 14. Rameix-Welti MA, Le Goffic R, Herve PL, Sourimant J, Remot A, Riffault S, et al. Visualizing the replication of respiratory syncytial virus in cells and in living mice. *Nat Commun*. 2014; 5:5104. doi: [10.1038/ncomms6104](https://doi.org/10.1038/ncomms6104) PMID: [25277263](https://pubmed.ncbi.nlm.nih.gov/25277263/).
 15. Peebles RS Jr., Graham BS. Pathogenesis of respiratory syncytial virus infection in the murine model. *Proc Am Thorac Soc*. 2005; 2(2):110–5. doi: [10.1513/pats.200501-002AW](https://doi.org/10.1513/pats.200501-002AW) PMID: [16113477](https://pubmed.ncbi.nlm.nih.gov/16113477/); PubMed Central PMCID: [PMC2713314](https://pubmed.ncbi.nlm.nih.gov/PMC2713314/).
 16. Graham BS, Perkins MD, Wright PF, Karzon DT. Primary respiratory syncytial virus infection in mice. *J Med Virol*. 1988; 26(2):153–62. Epub 1988/10/01. PMID: [3183639](https://pubmed.ncbi.nlm.nih.gov/3183639/).
 17. Rutigliano JA, Ruckwardt TJ, Martin JE, Graham BS. Relative dominance of epitope-specific CD8+ T cell responses in an F1 hybrid mouse model of respiratory syncytial virus infection. *Virology*. 2007; 362(2):314–9. Epub 2007/02/06. doi: [S0042-6822\(06\)00895-6](https://doi.org/S0042-6822(06)00895-6) [pii] doi: [10.1016/j.virol.2006.12.023](https://doi.org/10.1016/j.virol.2006.12.023) PMID: [17275872](https://pubmed.ncbi.nlm.nih.gov/17275872/); PubMed Central PMCID: [PMC1950131](https://pubmed.ncbi.nlm.nih.gov/PMC1950131/).
 18. Simmons CP, Hussell T, Sparer T, Walzl G, Openshaw P, Dougan G. Mucosal delivery of a respiratory syncytial virus CTL peptide with enterotoxin-based adjuvants elicits protective, immunopathogenic, and immunoregulatory antiviral CD8+ T cell responses. *J Immunol*. 2001; 166(2):1106–13. Epub 2001/01/06. PMID: [11145691](https://pubmed.ncbi.nlm.nih.gov/11145691/).
 19. Ostler T, Davidson W, Ehl S. Virus clearance and immunopathology by CD8(+) T cells during infection with respiratory syncytial virus are mediated by IFN-gamma. *Eur J Immunol*. 2002; 32(8):2117–23. Epub 2002/09/05. doi: [10.1002/1521-4141\(200208\)32:8<2117::AID-IMMU2117>3.0.CO;2-C](https://doi.org/10.1002/1521-4141(200208)32:8<2117::AID-IMMU2117>3.0.CO;2-C) PMID: [12209623](https://pubmed.ncbi.nlm.nih.gov/12209623/).
 20. Ruckwardt TJ, Luongo C, Malloy AM, Liu J, Chen M, Collins PL, et al. Responses against a subdominant CD8+ T cell epitope protect against immunopathology caused by a dominant epitope. *J Immunol*. 2010; 185(8):4673–80. doi: [10.4049/jimmunol.1001606](https://doi.org/10.4049/jimmunol.1001606) PMID: [20833834](https://pubmed.ncbi.nlm.nih.gov/20833834/); PubMed Central PMCID: [PMC4144756](https://pubmed.ncbi.nlm.nih.gov/PMC4144756/).
 21. Anderson KG, Sung H, Skon CN, Lefrancois L, Deisinger A, Vezys V, et al. Cutting edge: intravascular staining redefines lung CD8 T cell responses. *J Immunol*. 2012; 189(6):2702–6. doi: [10.4049/jimmunol.1201682](https://doi.org/10.4049/jimmunol.1201682) PMID: [22896631](https://pubmed.ncbi.nlm.nih.gov/22896631/); PubMed Central PMCID: [PMC3436991](https://pubmed.ncbi.nlm.nih.gov/PMC3436991/).
 22. Teijaro JR, Turner D, Pham Q, Wherry EJ, Lefrancois L, Farber DL. Cutting edge: Tissue-retentive lung memory CD4 T cells mediate optimal protection to respiratory virus infection. *J Immunol*. 2011; 187(11):5510–4. doi: [10.4049/jimmunol.1102243](https://doi.org/10.4049/jimmunol.1102243) PMID: [22058417](https://pubmed.ncbi.nlm.nih.gov/22058417/); PubMed Central PMCID: [PMC3221837](https://pubmed.ncbi.nlm.nih.gov/PMC3221837/).
 23. Ruckwardt TJ, Malloy AM, Gostick E, Price DA, Dash P, McClaren JL, et al. Neonatal CD8 T-cell hierarchy is distinct from adults and is influenced by intrinsic T cell properties in respiratory syncytial virus infected mice. *PLoS Pathog*. 7(12):e1002377. Epub 2011/12/07. doi: [10.1371/journal.ppat.1002377](https://doi.org/10.1371/journal.ppat.1002377) PPATHOGENS-D-11-01551 [pii]. PMID: [22144888](https://pubmed.ncbi.nlm.nih.gov/22144888/); PubMed Central PMCID: [PMC3228797](https://pubmed.ncbi.nlm.nih.gov/PMC3228797/).
 24. Coles RM, Mueller SN, Heath WR, Carbone FR, Brooks AG. Progression of armed CTL from draining lymph node to spleen shortly after localized infection with herpes simplex virus 1. *J Immunol*. 2002; 168(2):834–8. Epub 2002/01/05. PMID: [11777979](https://pubmed.ncbi.nlm.nih.gov/11777979/).
 25. Hu G, Chen J. A genome-wide regulatory network identifies key transcription factors for memory CD8 (+) T-cell development. *Nat Commun*. 2013; 4:2830. doi: [10.1038/ncomms3830](https://doi.org/10.1038/ncomms3830) PMID: [24335726](https://pubmed.ncbi.nlm.nih.gov/24335726/); PubMed Central PMCID: [PMC3999894](https://pubmed.ncbi.nlm.nih.gov/PMC3999894/).
 26. Farber DL, Yudanin NA, Restifo NP. Human memory T cells: generation, compartmentalization and homeostasis. *Nat Rev Immunol*. 2014; 14(1):24–35. doi: [10.1038/nri3567](https://doi.org/10.1038/nri3567) PMID: [24336101](https://pubmed.ncbi.nlm.nih.gov/24336101/); PubMed Central PMCID: [PMC4032067](https://pubmed.ncbi.nlm.nih.gov/PMC4032067/).

27. Best JA, Blair DA, Knell J, Yang E, Mayya V, Doedens A, et al. Transcriptional insights into the CD8(+) T cell response to infection and memory T cell formation. *Nat Immunol.* 2013; 14(4):404–12. doi: [10.1038/ni.2536](https://doi.org/10.1038/ni.2536) PMID: [23396170](https://pubmed.ncbi.nlm.nih.gov/23396170/); PubMed Central PMCID: PMC3689652.
28. Paley MA, Kroy DC, Odorizzi PM, Johnnidis JB, Dolfi DV, Barnett BE, et al. Progenitor and terminal subsets of CD8+ T cells cooperate to contain chronic viral infection. *Science.* 2012; 338(6111):1220–5. doi: [10.1126/science.1229620](https://doi.org/10.1126/science.1229620) PMID: [23197535](https://pubmed.ncbi.nlm.nih.gov/23197535/); PubMed Central PMCID: PMC3653769.
29. Wherry EJ. T cell exhaustion. *Nat Immunol.* 2011; 12(6):492–9. PMID: [21739672](https://pubmed.ncbi.nlm.nih.gov/21739672/).
30. Pagan JK, Arnold J, Hanchard KJ, Kumar R, Bruno T, Jones MJ, et al. A novel corepressor, BCoR-L1, represses transcription through an interaction with CtBP. *J Biol Chem.* 2007; 282(20):15248–57. Epub 2007/03/24. doi: [10.1074/jbc.M700246200](https://doi.org/10.1074/jbc.M700246200) [pii] doi: [10.1074/jbc.M700246200](https://pubmed.ncbi.nlm.nih.gov/17379597/) PMID: [17379597](https://pubmed.ncbi.nlm.nih.gov/17379597/).
31. Huynh KD, Fischle W, Verdin E, Bardwell VJ. BCoR, a novel corepressor involved in BCL-6 repression. *Genes Dev.* 2000; 14(14):1810–23. Epub 2000/07/18. PMID: [10898795](https://pubmed.ncbi.nlm.nih.gov/10898795/); PubMed Central PMCID: PMC316791.
32. Krona C, Ejekkar K, Caren H, Abel F, Sjoberg RM, Martinsson T. A novel 1p36.2 located gene, APITD1, with tumour-suppressive properties and a putative p53-binding domain, shows low expression in neuroblastoma tumours. *Br J Cancer.* 2004; 91(6):1119–30. Epub 2004/08/26. doi: [10.1038/sj.bjc.6602083](https://doi.org/10.1038/sj.bjc.6602083) 6602083 [pii]. PMID: [15328517](https://pubmed.ncbi.nlm.nih.gov/15328517/); PubMed Central PMCID: PMC2747717.
33. Boyd JM, Gallo GJ, Elangovan B, Houghton AB, Malstrom S, Avery BJ, et al. Bik, a novel death-inducing protein shares a distinct sequence motif with Bcl-2 family proteins and interacts with viral and cellular survival-promoting proteins. *Oncogene.* 1995; 11(9):1921–8. Epub 1995/11/02. PMID: [7478623](https://pubmed.ncbi.nlm.nih.gov/7478623/).
34. Ghavami S, Hashemi M, Ande SR, Yeganeh B, Xiao W, Eshraghi M, et al. Apoptosis and cancer: mutations within caspase genes. *J Med Genet.* 2009; 46(8):497–510. Epub 2009/06/10. doi: [10.1136/jmg.2009.066944](https://doi.org/10.1136/jmg.2009.066944) [pii] doi: [10.1136/jmg.2009.066944](https://pubmed.ncbi.nlm.nih.gov/19505876/) PMID: [19505876](https://pubmed.ncbi.nlm.nih.gov/19505876/).
35. Prasad KV, Ao Z, Yoon Y, Wu MX, Rizk M, Jacquot S, et al. CD27, a member of the tumor necrosis factor receptor family, induces apoptosis and binds to Siva, a proapoptotic protein. *Proc Natl Acad Sci U S A.* 1997; 94(12):6346–51. Epub 1997/06/10. PMID: [9177220](https://pubmed.ncbi.nlm.nih.gov/9177220/); PubMed Central PMCID: PMC21052.
36. Wu M, Xu LG, Li X, Zhai Z, Shu HB. AMID, an apoptosis-inducing factor-homologous mitochondrion-associated protein, induces caspase-independent apoptosis. *J Biol Chem.* 2002; 277(28):25617–23. Epub 2002/05/01. doi: [10.1074/jbc.M202285200](https://doi.org/10.1074/jbc.M202285200) M202285200 [pii]. PMID: [11980907](https://pubmed.ncbi.nlm.nih.gov/11980907/).
37. Shibahara K, Asano M, Ishida Y, Aoki T, Koike T, Honjo T. Isolation of a novel mouse gene MA-3 that is induced upon programmed cell death. *Gene.* 1995; 166(2):297–301. Epub 1995/12/12. doi: [10.1016/0378111995006079](https://doi.org/10.1016/0378111995006079) [pii]. PMID: [8543179](https://pubmed.ncbi.nlm.nih.gov/8543179/).
38. Bergametti F, Denier C, Labauge P, Arnoult M, Boetto S, Clanet M, et al. Mutations within the programmed cell death 10 gene cause cerebral cavernous malformations. *Am J Hum Genet.* 2005; 76(1):42–51. Epub 2004/11/16. doi: [10.1086/426952](https://doi.org/10.1086/426952) S0002-9297(07)62542-7 [pii] doi: [10.1086/426952](https://pubmed.ncbi.nlm.nih.gov/15543491/) PMID: [15543491](https://pubmed.ncbi.nlm.nih.gov/15543491/); PubMed Central PMCID: PMC1196432.
39. Satterwhite E, Sonoki T, Willis TG, Harder L, Nowak R, Arriola EL, et al. The BCL11 gene family: involvement of BCL11A in lymphoid malignancies. *Blood.* 2001; 98(12):3413–20. Epub 2001/11/24. PMID: [11719382](https://pubmed.ncbi.nlm.nih.gov/11719382/).
40. Baron BW, Anastasi J, Thirman MJ, Furukawa Y, Fears S, Kim DC, et al. The human programmed cell death-2 (PDCD2) gene is a target of BCL6 repression: implications for a role of BCL6 in the down-regulation of apoptosis. *Proc Natl Acad Sci U S A.* 2002; 99(5):2860–5. Epub 2002/02/21. doi: [10.1073/pnas.042702599](https://doi.org/10.1073/pnas.042702599) 042702599 [pii]. PMID: [11854457](https://pubmed.ncbi.nlm.nih.gov/11854457/); PubMed Central PMCID: PMC122438.
41. Hitoshi Y, Lorens J, Kitada SI, Fisher J, LaBarge M, Ring HZ, et al. Toso, a cell surface, specific regulator of Fas-induced apoptosis in T cells. *Immunity.* 1998; 8(4):461–71. Epub 1998/05/20. doi: [10.1016/S1074-7613\(00\)80551-8](https://doi.org/10.1016/S1074-7613(00)80551-8) [pii]. PMID: [9586636](https://pubmed.ncbi.nlm.nih.gov/9586636/).
42. Hansen SG, Piatak M Jr., Ventura AB, Hughes CM, Gilbride RM, Ford JC, et al. Immune clearance of highly pathogenic SIV infection. *Nature.* 2013; 502(7469):100–4. doi: [10.1038/nature12519](https://doi.org/10.1038/nature12519) PMID: [24025770](https://pubmed.ncbi.nlm.nih.gov/24025770/); PubMed Central PMCID: PMC3849456.
43. Aung S, Rutigliano JA, Graham BS. Alternative mechanisms of respiratory syncytial virus clearance in perforin knockout mice lead to enhanced disease. *J Virol.* 2001; 75(20):9918–24. Epub 2001/09/18. doi: [10.1128/JVI.75.20.9918-9924.2001](https://doi.org/10.1128/JVI.75.20.9918-9924.2001) PMID: [11559824](https://pubmed.ncbi.nlm.nih.gov/11559824/); PubMed Central PMCID: PMC114563.
44. Chang J, Braciale TJ. Respiratory syncytial virus infection suppresses lung CD8+ T-cell effector activity and peripheral CD8+ T-cell memory in the respiratory tract. *Nat Med.* 2002; 8(1):54–60. Epub 2002/01/12. doi: [10.1038/nm0102-54](https://doi.org/10.1038/nm0102-54) nm0102-54 [pii]. PMID: [11786907](https://pubmed.ncbi.nlm.nih.gov/11786907/).
45. Schenkel JM, Fraser KA, Vezys V, Masopust D. Sensing and alarm function of resident memory CD8(+) T cells. *Nat Immunol.* 2013; 14(5):509–13. doi: [10.1038/ni.2568](https://doi.org/10.1038/ni.2568) PMID: [23542740](https://pubmed.ncbi.nlm.nih.gov/23542740/); PubMed Central PMCID: PMC3631432.

46. Knudson CJ, Weiss KA, Hartwig SM, Varga SM. The pulmonary localization of virus-specific T lymphocytes is governed by the tissue tropism of infection. *J Virol.* 2014; 88(16):9010–6. doi: [10.1128/JVI.00329-14](https://doi.org/10.1128/JVI.00329-14) PMID: [24899187](https://pubmed.ncbi.nlm.nih.gov/24899187/); PubMed Central PMCID: PMC4136240.
47. Alexander-Miller MA, Leggatt GR, Berzofsky JA. Selective expansion of high- or low-avidity cytotoxic T lymphocytes and efficacy for adoptive immunotherapy. *Proc Natl Acad Sci U S A.* 1996; 93(9):4102–7. Epub 1996/04/30. PMID: [8633023](https://pubmed.ncbi.nlm.nih.gov/8633023/); PubMed Central PMCID: PMC39494.
48. Messaoudi I, Guevara Patino JA, Dyall R, LeMaout J, Nikolich-Zugich J. Direct link between mhc polymorphism, T cell avidity, and diversity in immune defense. *Science.* 2002; 298(5599):1797–800. Epub 2002/12/03. doi: [10.1126/science.1076064](https://doi.org/10.1126/science.1076064) 298/5599/1797 [pii]. PMID: [12459592](https://pubmed.ncbi.nlm.nih.gov/12459592/).
49. Billam P, Bonaparte KL, Liu J, Ruckwardt TJ, Chen M, Ryder AB, et al. T Cell receptor clonotype influences epitope hierarchy in the CD8+ T cell response to respiratory syncytial virus infection. *J Biol Chem.* 286(6):4829–41. Epub 2010/12/02. doi: M110.191437 [pii] doi: [10.1074/jbc.M110.191437](https://doi.org/10.1074/jbc.M110.191437) PMID: [21118816](https://pubmed.ncbi.nlm.nih.gov/21118816/); PubMed Central PMCID: PMC3039322.
50. Turner SJ, La Gruta NL, Kedzierska K, Thomas PG, Doherty PC. Functional implications of T cell receptor diversity. *Curr Opin Immunol.* 2009; 21(3):286–90. doi: [10.1016/j.coi.2009.05.004](https://doi.org/10.1016/j.coi.2009.05.004) PMID: [19524428](https://pubmed.ncbi.nlm.nih.gov/19524428/); PubMed Central PMCID: PMC2706259.
51. Hansen SG, Vieville C, Whizin N, Coyne-Johnson L, Siess DC, Drummond DD, et al. Effector memory T cell responses are associated with protection of rhesus monkeys from mucosal simian immunodeficiency virus challenge. *Nat Med.* 2009; 15(3):293–9. Epub 2009/02/17. doi: nm.1935 [pii] doi: [10.1038/nm.1935](https://doi.org/10.1038/nm.1935) PMID: [19219024](https://pubmed.ncbi.nlm.nih.gov/19219024/); PubMed Central PMCID: PMC2720091.
52. Buchholz VR, Flossdorf M, Hensel I, Kretschmer L, Weissbrich B, Graf P, et al. Disparate individual fates compose robust CD8+ T cell immunity. *Science.* 2013; 340(6132):630–5. doi: [10.1126/science.1235454](https://doi.org/10.1126/science.1235454) PMID: [23493420](https://pubmed.ncbi.nlm.nih.gov/23493420/).
53. Obar JJ, Khanna KM, Lefrancois L. Endogenous naive CD8+ T cell precursor frequency regulates primary and memory responses to infection. *Immunity.* 2008; 28(6):859–69. Epub 2008/05/24. doi: S1074-7613(08)00200-8 [pii] doi: [10.1016/j.immuni.2008.04.010](https://doi.org/10.1016/j.immuni.2008.04.010) PMID: [18499487](https://pubmed.ncbi.nlm.nih.gov/18499487/); PubMed Central PMCID: PMC2836785.
54. Kotturi MF, Scott I, Wolfe T, Peters B, Sidney J, Cheroutre H, et al. Naive precursor frequencies and MHC binding rather than the degree of epitope diversity shape CD8+ T cell immunodominance. *J Immunol.* 2008; 181(3):2124–33. Epub 2008/07/22. doi: 181/3/2124 [pii]. PMID: [18641351](https://pubmed.ncbi.nlm.nih.gov/18641351/); PubMed Central PMCID: PMC3319690.
55. Labrecque N, Whitfield LS, Obst R, Waltzinger C, Benoist C, Mathis D. How much TCR does a T cell need? *Immunity.* 2001; 15(1):71–82. PMID: [11485739](https://pubmed.ncbi.nlm.nih.gov/11485739/).
56. Leignadier J, Rooney J, Daudelin JF, Labrecque N. Lowering TCR expression on naive CD8+ T cells does not affect memory T-cell differentiation. *Immunol Cell Biol.* 2011; 89(2):322–5. doi: [10.1038/icb.2010.80](https://doi.org/10.1038/icb.2010.80) PMID: [20585337](https://pubmed.ncbi.nlm.nih.gov/20585337/).
57. de Bree GJ, van Leeuwen EM, Out TA, Jansen HM, Jonkers RE, van Lier RA. Selective accumulation of differentiated CD8+ T cells specific for respiratory viruses in the human lung. *J Exp Med.* 2005; 202(10):1433–42. Epub 2005/11/23. doi: jem.20051365 [pii] doi: [10.1084/jem.20051365](https://doi.org/10.1084/jem.20051365) PMID: [16301748](https://pubmed.ncbi.nlm.nih.gov/16301748/); PubMed Central PMCID: PMC2212987.
58. Liu J, Ruckwardt TJ, Chen M, Nicewonger JD, Johnson TR, Graham BS. Epitope-specific regulatory CD4 T cells reduce virus-induced illness while preserving CD8 T-cell effector function at the site of infection. *J Virol.* 84(20):10501–9. Epub 2010/08/06. doi: JVI.00963-10 [pii] doi: [10.1128/JVI.00963-10](https://doi.org/10.1128/JVI.00963-10) PMID: [20686045](https://pubmed.ncbi.nlm.nih.gov/20686045/); PubMed Central PMCID: PMC2950556.
59. Erickson JJ, Gilchuk P, Hastings AK, Tollefson SJ, Johnson M, Downing MB, et al. Viral acute lower respiratory infections impair CD8+ T cells through PD-1. *J Clin Invest.* 2012; 122(8):2967–82. doi: [10.1172/JCI62860](https://doi.org/10.1172/JCI62860) PMID: [22797302](https://pubmed.ncbi.nlm.nih.gov/22797302/); PubMed Central PMCID: PMC3408742.
60. Telcian AG, Laza-Stanca V, Edwards MR, Harker JA, Wang H, Bartlett NW, et al. RSV-induced bronchial epithelial cell PD-L1 expression inhibits CD8+ T cell nonspecific antiviral activity. *J Infect Dis.* 203(1):85–94. Epub 2010/12/15. doi: jiq020 [pii] doi: [10.1093/infdis/jiq020](https://doi.org/10.1093/infdis/jiq020) PMID: [21148500](https://pubmed.ncbi.nlm.nih.gov/21148500/); PubMed Central PMCID: PMC3086441.
61. Hogan RJ, Usherwood EJ, Zhong W, Roberts AA, Dutton RW, Harmsen AG, et al. Activated antigen-specific CD8+ T cells persist in the lungs following recovery from respiratory virus infections. *J Immunol.* 2001; 166(3):1813–22. Epub 2001/02/13. PMID: [11160228](https://pubmed.ncbi.nlm.nih.gov/11160228/).
62. De Jong R, Brouwer M, Hooibrink B, Van der Pouw-Kraan T, Miedema F, Van Lier RA. The CD27- subset of peripheral blood memory CD4+ lymphocytes contains functionally differentiated T lymphocytes that develop by persistent antigenic stimulation in vivo. *Eur J Immunol.* 1992; 22(4):993–9. Epub 1992/04/01. doi: [10.1002/eji.1830220418](https://doi.org/10.1002/eji.1830220418) PMID: [1348033](https://pubmed.ncbi.nlm.nih.gov/1348033/).

63. Linsley PS, Bradshaw J, Urnes M, Grosmaire L, Ledbetter JA. CD28 engagement by B7/BB-1 induces transient down-regulation of CD28 synthesis and prolonged unresponsiveness to CD28 signaling. *J Immunol.* 1993; 150(8 Pt 1):3161–9. Epub 1993/04/15. PMID: [7682233](#).
64. Gamadia LE, van Leeuwen EM, Remmerswaal EB, Yong SL, Surachno S, Wertheim-van Dillen PM, et al. The size and phenotype of virus-specific T cell populations is determined by repetitive antigenic stimulation and environmental cytokines. *J Immunol.* 2004; 172(10):6107–14. Epub 2004/05/07. PMID: [15128796](#).
65. Kaech SM, Tan JT, Wherry EJ, Konieczny BT, Surh CD, Ahmed R. Selective expression of the interleukin 7 receptor identifies effector CD8 T cells that give rise to long-lived memory cells. *Nat Immunol.* 2003; 4(12):1191–8. Epub 2003/11/20. doi: [10.1038/ni1009](#) ni1009 [pii]. PMID: [14625547](#).
66. van Leeuwen EM, de Bree GJ, Remmerswaal EB, Yong SL, Tesselaar K, ten Berge IJ, et al. IL-7 receptor alpha chain expression distinguishes functional subsets of virus-specific human CD8+ T cells. *Blood.* 2005; 106(6):2091–8. Epub 2005/06/11. doi: 2005-02-0449 [pii] doi: [10.1182/blood-2005-02-0449](#) PMID: [15947093](#).
67. Melenhorst JJ, Scheinberg P, Chattopadhyay PK, Lissina A, Gostick E, Cole DK, et al. Detection of low avidity CD8(+) T cell populations with coreceptor-enhanced peptide-major histocompatibility complex class I tetramers. *Journal of immunological methods.* 2008; 338(1–2):31–9. doi: [10.1016/j.jim.2008.07.008](#) PMID: [18675271](#); PubMed Central PMCID: PMC2714739.